

Surface Motion of Alluvial Valleys Subjected to Obliquely Incident Plane *SH*-Wave Propagation

Mehdi Panji & Saeed Mojtazadeh-Hasanlouei

To cite this article: Mehdi Panji & Saeed Mojtazadeh-Hasanlouei (2021): Surface Motion of Alluvial Valleys Subjected to Obliquely Incident Plane *SH*-Wave Propagation, Journal of Earthquake Engineering, DOI: [10.1080/13632469.2021.1927886](https://doi.org/10.1080/13632469.2021.1927886)

To link to this article: <https://doi.org/10.1080/13632469.2021.1927886>



Published online: 26 May 2021.



Submit your article to this journal [↗](#)





View related articles [↗](#)



View Crossmark data [↗](#)



Surface Motion of Alluvial Valleys Subjected to Obliquely Incident Plane *SH*-Wave Propagation

Mehdi Panji  and Saeed Mojtabazadeh-Hasanlouei 

Department of Civil Engineering, Zanjan Branch, Islamic Azad University, Zanjan, Iran

ABSTRACT

In this paper, a simple numerical model is presented for analyzing arbitrarily shaped alluvial valleys subjected to propagating obliquely incident plane *SH*-waves. A time-domain half-plane boundary element method (BEM) was successfully used to prepare the model in which the interface needs only to be discretized. First, the problem was decomposed into two parts, a half-plane valley-shaped feature and a closed filled alluvium. Then, the method was applied to each part to obtain the considered matrices. Finally, by satisfying the continuity conditions at the interface, the coupled equation was transiently solved to determine the boundary values. All ground surface responses were also obtained in a secondary solution as internal points. After implementing the method in a general algorithm, several practical examples were analyzed to validate the responses. Moreover, an advanced numerical study was performed to sensitize the surface motion of semi-cylindrical alluvial valleys with variable shape ratios as synthetic seismograms and three-dimensional (3D) amplification patterns. The proposed method can easily be combined with other numerical methods to achieve nonlinear site responses.

ARTICLE HISTORY

Received 5 February 2019
Accepted 29 April 2021

KEYWORDS

Alluvial valley; Half-plane BEM; Synthetic seismogram; *SH*-wave; Time-domain

1. Introduction

In the last decades, the behavior of alluvial valleys in seismic mode and their important role in the amplifications/de-amplifications of ground surface responses have been recognized by seismologists and engineers as major topics, reflected in some seismic codes (Aki 1988; Davis and West 1973; Sánchez-Sesma 1987). Therefore, numerous studies focused on the effective parameters of alluviums and damage investigations in their gamut during earthquakes (Aki 1993; Bard and Bouchon 1980a, 1980b; Manoogian and Lee 1999). This phenomenon may be due to various factors such as local conditions and quality of constructions, effects of topographic features, superficial soil characteristics, and local geological behaviors (Wong and Trifunac 1974a). In this way, various approaches have been applied by numerous authors to model and analyze the problems of wave scattering for predicting the real responses of alluvial valleys. All these efforts were made to determine reliable design parameters and decrease damages as much as possible (Esteva 1977), providing a new insight into the behavior of alluviums and clarifying the basic aspects of this problem (Aki and Larner 1970; Boore 1972; Bouchon 1973; Trifunac 1971, 1973; Wong and Trifunac 1974a).

From a technical point of view, these approaches can be divided into analytical, semi-analytical, experimental, and numerical methods, each with certain advantages and disadvantages (Sánchez-Sesma, Palencia, and Luzón 2002). In the use of analytical and semi-analytical approaches, the analysis process will be highly complicated due to the low flexibility and high complexity of equations,

CONTACT Mehdi Panji  m.panji@iauz.ac.ir  Department of Civil Engineering, Zanjan Branch, Islamic Azad University, Zanjan, Iran.

Mehdi Panji proposed the basic idea, performed the formulation and implemented it into his comprehensive advanced algorithm previously named DASBEM. Saeed Mojtabazadeh-Hasanlouei prepared the numerical models, performed the advanced parametric study and graphical processing of the figures.

especially for complex problems and geometries. For this reason, the use of analytical and semi-analytical methods is limited to the simple models. On the other hand, the achieved responses from these methods are very accurate. The pioneering studies by analytical and semi-analytical methods on the seismic behavior of alluvial valleys and canyons were conducted in the early 1970s, including the analytical study by Trifunac (1971), Trifunac (1973), Wong and Trifunac (1974a), Wong and Trifunac (1974b). Lee (1984) studied the three-dimensional (3D) diffraction of plane P , SV , and SH -waves in the presence of a hemispherical alluvial valley. Todorovska and Lee (1991) investigated the surface motion of shallow circular alluvial valleys. The 2D scattering of plane SH -waves by a cylindrical alluvial valley was addressed by Yuan and Liao (1995). Sherif and Lee (1996) investigated the wave propagation behavior around a circular alluvial valley placed subjected to SH -waves. Weihua, Chenggang, and Peixin (2005) proposed an analytical solution for the scattering of plane P -waves due to circular-arc alluvial valleys placed in saturated soil. The diffraction of plane P -waves by a hemispherical alluvial valley placed in saturated soil was presented by Gao, Zhao, and Dong (2006). Then, Tsaur and Chang (2008a) and Tsaur and Chang (2009) studied the scattering of SH -waves in the presence of a partially filled semi-circular alluvial valleys and canyons. Faik-Kara and Trifunac (2013) proposed a note for plane-wave approximation, followed by Jalali, Tokmechi, and Trifunac (2015) were presented a note for surface motion determination in the presence of a semi-cylindrical alluvial valley subjected to SH -waves. In another study, Faik-Kara and Trifunac (2014) investigated on the earthquake vibration effect due to SH -waves on sedimentary basins. Some other researchers such as Zhang et al. (2012), Chang, Tsaur, and Wang (2013) and Chang, Tsaur, and Wang (2015) were focused on the problem of asymmetrical canyons. Using wave function expansion method, Zhang, Gao, and Pak (2017) and Le, Lee, and Trifunac (2017) studied the SH -waves scattering in the presence the semi-cylindrical and moon-shaped valleys, respectively. Recently, Tsaur and Chang (2018) were able to propose an exact solution for the scattering of SH -waves in the presence of an elliptic-arc canyon analytically. In these studies, the wave function expansion method was utilized.

Due to the mentioned limitations of analytical and semi-analytical methods in the modeling of complex geometries, the use of numerical methods became inevitable (Sánchez-Sesma and Rosenblueth 1979). For example, Sánchez-Sesma and Esquivel (1979) focused on the motions of the ground surface in the presence of alluvial valleys subjected to incident plane SH -waves. The wave amplification by two alluvial valleys subjected to P and SV -waves was addressed by Dravinski (1983). The mentioned studies were formulated by Fredholm integral equations and a boundary integral method, respectively, and were then numerically solved. By the development and improvement of computing devices in recent decades, numerical methods have received more attention from researchers. This category of approaches has been developed in different branches of domain and boundary methods. The finite-element method (FEM) and finite-difference method (FDM) are known as the main domain methods. When domain methods are employed, the domain of the problem should be discretized and the energy absorber boundaries should be considered. These circumstances are inseparable parts of modeling and analysis in both infinite and semi-infinite continuous media. Thus, this can increase the complexity of problems and lead to a longer analysis time. Studies of Lysmer and Drake (1972), Smith (1975), Kawase and Sato (1992), and Bielak, Xu, and Ghattas (1999) are the pioneering investigations using FEM. In these studies, they highlighted the application of the mentioned method in seismology, developed the analytical approaches of body wave propagation and examined the ground surface motion during an earthquake and structural seismic responses in presence of alluvial valleys, respectively. Recently, Nohegoo-Shahvari, Kamalian, and Panji (2018, 2019) introduced a 2D seismic analysis of an alluvial valley subjected to vertically incident SH -waves by FEM. Using FDM, Frankel and Vidale (1992) were simulated the seismic waves in the Santa-Clara valley. The wave diffraction, amplification and differential surface motion near the strong lateral discontinuities were presented by Moczo and Bard (1993). Moreover, the response of an irregular free surface based on the traction image technique and scattering of SH -waves were presented by Zhang and Chen (2006) and Zhou and Chen (2006), respectively. Wang et al. (2015) investigated the effect of near-surface topographic features subjected to the high-frequency Rayleigh waves by FDM.

Furthermore, Komatitsch and Vilotte (1998) and Paolucci (2002) simulated the seismic responses of 2D/3D geological structures and explored the amplification of earthquakes on ground surface by steep topographic features using the spectral-element method. Also, the seismic response of rectangular alluvial valleys due to incident *SV*-waves was presented by Najafzadeh et al. (2014) using the same approach. Other researchers combined two or more approaches and used their benefits for modeling and analyses. These approaches are known as hybrid methods. For example, using an indirect boundary element/discrete wavenumber, Gil-Zepeda et al. (2003) were able to simulate the seismic response of stratified alluvial valleys. Also, the seismic site effect for 2D topographical irregularities and the behavior of sedimentary valleys were explored by Gatmiri, Arson, and Nguyen (2008a) and Gatmiri and Arson (2008b) with a 2D FEM/BEM approach.

Using boundary approaches, one dimension will be reduced in modeling, and Sommerfeld's radiation conditions will be satisfied at infinity for wave dispersion. These methods concentrate the meshes only around the boundary of valley-shaped topography and the content of alluvium placed inside the mentioned valley. This method is divided into two categories of direct boundary element method (DBEM) and indirect boundary element method (IBEM), but DBEM was further developed and researchers have been more willing to take advantage of it. By utilizing boundary element method (BEM), one dimension of the models will be reduced and the radiation conditions of waves at infinity will be satisfied. The advantages of using boundary element method (BEM) compared to the domain approaches include concentration of meshes only around the boundary of desired topographic features, automatic satisfaction of wave radiation conditions in far boundaries, lower volume of input data, significant reduction in occupied memory and analysis time beside extremely high accuracy of exported results because of the large contribution of analytical processes in solving problems (Kamalian et al. 2007). In addition, DBEM can be divided into two categories of full-plane and half-plane, each being developed in frequency and time-domain. This approach can also be used in static (Panji and Ansari 2017a; Panji, Asgari Marnani, and Tavousi Tafreshi 2011; Panji et al. 2016) and dynamic modes (Panji and Ansari 2017b) based on the definition of different problems. The implementation of the formulation will be more difficult in half-plane BEM compared to full-plane BEM due to the satisfaction of ground surface boundary condition in the formulation. In half-plane BEM, there is no need to discretize the surface and define fictitious elements on the side boundaries, making the models simpler. Sánchez-Sesma and Rosenblueth (1979) conducted a basic study using half-plane frequency-domain BEM and presented the ground motion due to arbitrarily shaped canyons and incident *SH*-waves. Then, the 3D responses of a cylindrical canyon in a layered half-space were obtained by Luco, Wong, and De Barros (1990), and the responses of the Mexico City valley with a 2D BEM due to *SH*-waves were illustrated by Reinoso, Wrobel, and Power (1993). The seismic responses of semi-elliptical alluvial valleys due to incident *SH*, *P*, and *SV*-waves were also presented by Fishman and Ahmad (1995). In another study, Sánchez-Sesma and Luzon (1995) discovered the seismic response of 3D alluvial valleys subjected to *P*, *S*, and Rayleigh waves using the half-plane indirect BEM approach. Utilizing the same method, Luco and De Barros (1994) were studied the dynamic displacements of cylindrical cavity embedded in a half space. In this regard, some researchers, including Luco and Apsel (1983a, 1983b), Rajapakse and Wang (1993), Senjuntichai and Rajapakse (1994) and Hisada (1994a, 1994b), were able to present the Green's functions of isotropic, transversely isotropic and poroelastic half-space. A few years later, the seismic responses of alluvial valleys for incidence *SH*-waves were presented by Ausilio, Conte, and Dente (2008). Recently, using indirect boundary integral equation method, Huang et al. (2019), Liang et al. (2019) and Liu et al. (2019) studied the elastic wave scattering by twin lining tunnels, a hill and in layered half-space, respectively. All of the noted studies were performed using the half-plane frequency-domain BEM.

In recent years, upon the development of the half-plane time-domain BEM by some researchers such as Panji (2013) and Panji et al. (2013a), the seismic analysis of various topographic features has been performed with this approach. The seismic analysis of semi-sine shaped valleys subjected to vertically propagating incident *SH*-waves was performed by Panji et al. (2013b) using a half-plane time-domain BEM. A year after, the seismic response of convex topographies was examined by Panji et al. (2014a) using the mentioned approach. Also, the seismic response of a semi-sine shaped valley above an embedded truncated circular cavity was obtained by Panji et al. (2014b). Based on an indirect

BEM, the wave propagation of a complex local site in a layered half-space and the seismic response of alluvial valleys subjected to *SH*-waves were discovered by Ba and Yin (2016) and Ba and Liang (2017), respectively. Recently, Panji and Mojtabazadeh Hasanlouei (2018) illustrated the synthetic seismograms of the ground surface in the presence of regularly distributed enormous embedded cavities using a half-plane time-domain BEM. The seismic amplification pattern of the ground surface in presence of twin unlined circular tunnels subjected to *SH*-waves was presented by Panji and Mojtabazadeh-Hasanlouei (2019a). In another study, Panji and Mojtabazadeh-Hasanlouei (2019b) presented the transient response of irregular surface by periodically distributed semi-sine shaped valleys subjected to *SH*-waves. Moreover, the *SH*-wave dispersion by a single circular and elliptical inclusion was addressed by Panji, Mojtabazadeh-Hasanlouei, and Yasemi (2020).

The literature review shows that the scattering effect of transient *SH*-waves on the ground surface in the presence of alluvial valleys has not yet been directly analyzed in the time-domain by half-plane BEM. In previous researches, the models were limited to the homogeneous single-material subsurface problems. Although in some researches such as Lubich (1988), Garcia-Sanchez and Zhang (2007) and Manolis et al. (2017) etc., the mathematical formulation, numerical implementation and transient analysis of two-dimensional non-homogeneous solids were presented as well, they were established to obtain the time-domain responses by the inverse Fourier/Laplace-transform algorithm from mechanical problems point of view. Moreover, researchers like Takemiya and Fujiwara (1994) were able to present the time-domain responses for an alluvial valley, but they used full-plane time-domain BEM approach.

In this study, based on an advanced half-plane time-domain BEM, the surface response of a linear elastic alluvial valley is obtained due to propagating obliquely incident out-of-plane *SH*-waves. Although the proposed approach is classified in the group of numerical methods, it can be believed that this method is a kind of time-domain semi-analytical scheme because the closed-form transient kernels of the method have already been extracted. On the other hand, given that the actual behavior of the sedimentary basins is a non-linear response, it is necessary to analyze these features directly in the time-domain by a favorite approach. Therefore, in the present work, an efficient time-domain BEM is proposed to prepare a simple model of alluvial valleys by locating only a few nodes on the interface. Consequently, the analysis time, which is one of the problems of the transient solution in heterogeneous models, is significantly reduced. It is worth mentioning, unlike the other time-domain methods that the temporal integration is carried out in an approximate numerical process, the present results were stable against time-step changes due to the use of closed-form kernels. After developing the method to analyze the problem of the alluvial valley, it was implemented in a general algorithm previously called DASBEM¹ (Panji et al. 2013a). Then, a verification example was solved for the problem of a semi-circular alluvial valley to illustrate the accuracy and performance of the method. Next, the time-domain responses of the surface were obtained for semi-cylindrical alluvial valleys as synthetic seismograms in the form of a numerical study. Some key parameters, including the incident wave angle, depth ratio, and impedance ratio of the alluvium to the surrounding medium, were considered to sensitize the response behavior. Finally, the blanket amplification patterns were presented for some specific cases to demonstrate the frequency-domain responses. The main aim of this study was to reveal the power and accuracy of this developed algorithm in presenting time-domain responses for complicated engineering problems and present a better view of alluvial valleys' seismic behavior. The introduced method can be used by geotechnical/mechanical engineers to model the structures with arbitrarily shaped surfaces such as alluvial valleys in the fields of earthquake engineering and nanoscaled composite materials as well.

2. Problem Statement

As illustrated in Fig. 1, a linear elastic homogeneous and isotropic half-plane is considered as the medium of the models, and an alluvial valley is located in this medium. Therefore, based on Fig. 1, Γ is the boundary of the body defined separately for the valley and alluvium, DR represents the depth ratio of the valley, and b denotes the width of the valley. Moreover, Ω is the domain, and the subscripts 1 and 2 are related to the medium and alluvium, respectively. Also, θ is the angle of incidence waves, and parameter n is the normal

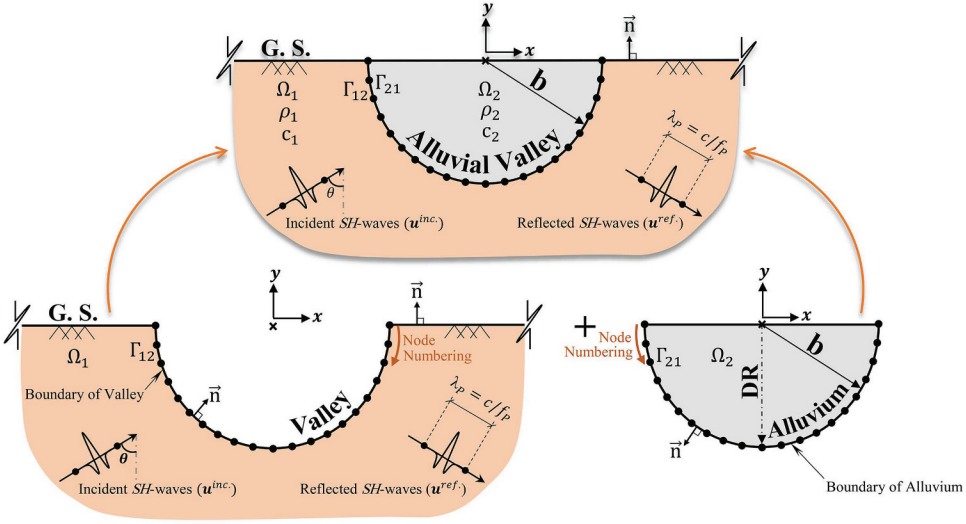


Figure 1. The problem geometry of an alluvial valley placed in an elastic half-plane subjected to incident SH -waves.

vector perpendicular to the surface and dependent on the node numbering direction. The models are subjected to incident out-of-plane SH -waves of the Ricker type (Panji et al. 2013a, 2013b). Figure 2 shows the diagrams of the Ricker wavelet for a point located on the free surface in time and frequency-domain, respectively. Moreover, the function of a Ricker wavelet type is defined as Eq. (1) (Ricker 1953):

$$f(t) = \left[1 - 2(\pi f_p(t - t_0))^2 \right] e^{-(\pi f_p(t - t_0))^2}, \quad (1)$$

In Eq. (1), f_p is the predominant frequency of the wave and t_0 is the time shift parameter. Since the modeling is completely conducted in half-plane and the stress-free boundary conditions of the ground surface are satisfied, free-field displacement (u^{ff}) can be obtainable by adding the phase of incident and reflected waves as follows (Reinoso, Wrobel, and Power 1993):

$$u^{ff}(x, y, t) = \alpha_{max} \left(\begin{array}{l} \left[1 - 2 \left(\frac{\pi f_p}{c} \alpha^{inc} \right)^2 \right] e^{-\left(\frac{\pi f_p}{c} \alpha^{inc} \right)^2} H \left(t - \frac{r^{inc}}{c} \right) + \\ \left[1 - 2 \left(\frac{\pi f_p}{c} \alpha^{ref} \right)^2 \right] e^{-\left(\frac{\pi f_p}{c} \alpha^{ref} \right)^2} H \left(t - \frac{r^{ref}}{c} \right) \end{array} \right), \quad (2)$$

where α^{inc} , α^{ref} , r^{inc} , and r^{ref} can be achieved from the following equations:

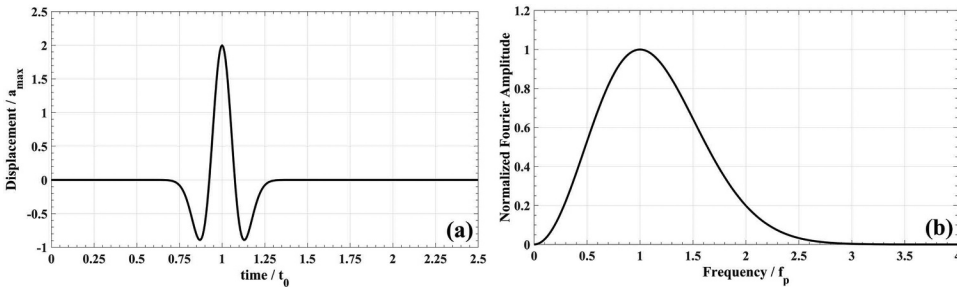


Figure 2. The diagram of the Ricker wavelet for a point located on free-field for (a) time-domain and (b) frequency-domain.

$$\alpha^{inc.} = c(t - t_0) + r^{inc.}, r^{inc.} = -\sin(\theta) \cdot x + \cos(\theta) \cdot y, \quad (3)$$

$$\alpha^{ref.} = c(t - t_0) + r^{ref.}, r^{ref.} = -\sin(\theta) \cdot x - \cos(\theta) \cdot y, \quad (4)$$

On the other hand, the equation of motion for the anti-plane strain model is as follows:

$$\frac{\partial^2 u(x, y, t)}{\partial x^2} + \frac{\partial^2 u(x, y, t)}{\partial y^2} + b(x, y, t) = \frac{1}{c^2} \frac{\partial^2 u(x, y, t)}{\partial t^2}, \quad (5)$$

In Eq. (5), $u(x, y, t)$ and $b(x, y, t)$ are out-of-plane displacement and body force at the point (x, y) and current time t , respectively. Furthermore, c is the shear-wave velocity determined by $\sqrt{\mu/\rho}$, in which μ is the shear modulus and ρ is the mass density. Regardless of any boundary condition on the singular solution of Eq. (5), the full-plane Green's functions were achieved (Israil and Banerjee 1990a, 1990b). However, to obtain a 2D anti-plane semi-infinite medium, Eq. (5) should be solved by the following boundary condition:

$$\left. \frac{\partial u(x, y, t)}{\partial n} \right|_{y=0} = 0, \quad (6)$$

By simultaneously taking the singular solution into account for Eqs. (5) and (6), the half-plane Green's functions can be obtained (Panji et al. 2013a).

3. Time-Domain Half-Plane Boundary Element Method (BEM)

Using the wave source image technique (Panji et al. 2013a) and satisfying the boundary conditions related to the ground surface, one can exclusively concentrate the meshes around the boundary of the valley. The details of this method are mentioned in the following section.

3.1. Boundary Integral Equation (BIE)

In the first step, without considering any boundary conditions of Eq. (6), the weighted residual integral was applied to Eq. (5). Then, by performing twice integration by parts, eliminating the volumetric integral defined on the domain using boundary methods, and ignoring the contributions of the initial conditions and body forces, the direct boundary integral equation (BIE) in the time-domain can be obtained as Eq. (7) (Brebbia and Dominguez 1989; Dominguez 1993; Reinoso, Wrobel, and Power 1993):

$$c(\xi)u(\xi, t) = \int_{\Gamma} \left\{ \int_0^t [u^*(x, t; \xi, \tau) \cdot q(x, t) - q^*(x, t; \xi, \tau) \cdot u(x, t)] d\tau \right\} d\Gamma(x), \quad (7)$$

In Eq. (7), u^* and q^* are the half-plane displacement and traction Green's functions of the time-domain, respectively (Panji et al. 2013a). Also, u and q are the displacements and traction fields on the boundary, respectively. Moreover, Γ denotes the boundary, and x and ξ depict the coordinates of source and receiver, respectively. Additionally, $u^* \cdot q$ and $q^* \cdot u$ are the Riemann-convolution integrals, and $c(\xi)$ represents the angle of boundary refraction defined as the geometry coefficient (Dominguez 1993). Then, to obtain the free-field displacement, by summing the incident and reflected wave-field, the BIE (Eq. (7)) can be modified to the following from (Hadley, Askar, and Cakmak 1989; Kawase 1988):

$$c(\xi)u(\xi, t) = \int_{\Gamma} \left\{ \int_0^t [u^*(x, t; \xi, \tau) \cdot q(x, t) - q^*(x, t; \xi, \tau) \cdot u(x, t)] d\tau \right\} d\Gamma(x) + u^{ff}(\xi, t), \quad (8)$$

where u^{ff} indicates the free-field displacement on the ground surface without the presence of any surface irregularities. By solving Eq. (8), the total displacement of the alluvial valley can be obtained. In this step, it is possible to obtain the displacements at any point m in Ω , including the ground surface ($y = 0$). The following modified equation can be used for internal points. In this step, $c^m(\xi)$ should be equal to 1.0.

$$u^m(\xi, t) = \int_{\Gamma} \left\{ \int_0^t [u^{*m}(x, t; \xi, \tau) \cdot q(x, t) - q^{*m}(x, t; \xi, \tau) \cdot u(x, t)] d\tau \right\} d\Gamma(x) + u^{ff.m}(\xi, t), \quad (9)$$

in which the half-plane displacement and traction Green's functions for each internal point are shown by u^{*m} and q^{*m} , respectively. Moreover, the free-field displacements are depicted by $u^{ff.m}$ which should be recalculated in this step.

4. Numerical Implementation

In this step, the time-axis should be considered and the geometric boundary of the body should be discretized before solving Eq. (8) and obtaining the field variables. In fact, the mentioned equation is an exact solution until reaching this step, and there is no approximation in this equation before applying the discretization on the boundaries of the valley and alluvium. To perform the temporal integration, the analytical process is required, and then the numerical procedure should be performed to achieve the spatial integration.

4.1. Temporal Integration

By considering Δt , the time interval will be divided into N equal increments from 0 to t , where $t = N\Delta t$, and the field variables can be assumed to remain linear within each time-step. By preparing the temporal integrations, the time-convoluted BIE can be rewritten as Eq. (10):

$$c(\xi)u^N(\xi) = \sum_{n=1}^N \int_{\Gamma} \left(\begin{array}{l} [U_1^{N-n+1}(x, \xi)q^n(x) + U_2^{N-n}(x, \xi)q^n(x)] - \\ [Q_1^{N-n+1}(x, \xi)u^n(x) + Q_2^{N-n}(x, \xi)u^n(x)] \end{array} \right) d\Gamma(x) + u^{ff.N}(\xi), \quad (10)$$

in which, U_1^{N-n+1} and U_2^{N-n} are the half-plane displacement time-convoluted kernels and Q_1^{N-n+1} and Q_2^{N-n} are the half-plane traction time-convoluted kernels. These kernels correspond to the forward and backward time-nodes within a time-step, shortened in the closed-form. The boundary displacement and free-field displacement are demonstrated as u^N and $u^{ff.N}$, respectively, at time $t = N\Delta t$. The full form of the time-convoluted kernels of anti-plane elastodynamics for half-plane displacement and traction is introduced by Panji et al. (2013a, 2014a).

4.2. Spatial Integration

The isoparametric quadratic elements are used to discretize the boundary of the domain for performing spatial integration in the numerical form, and all the quantities related to the geometry and field variables are given in terms of nodal variables.

$$x_i(\kappa) = N_a(\kappa)x_{ia}, \quad (11)$$

$$f(x(\kappa)) = N_a(\kappa)f_a, \quad (12)$$

In these equations, f is the displacement and traction, and $N_a(\kappa)$ is the quadratic shape functions in which κ is the local intrinsic coordinates of the elements. By considering the spatial discretization, Eq. (10) can be rewritten as Eq. (13):

$$c(\xi)u^N(\xi) = \sum_{n=1}^N \sum_{m=1}^M \left[\int_{\Gamma_m} [U_1^{N-n+1}(x(\kappa), \xi) + U_2^{N-n}(x(\kappa), \xi)] N_\alpha(\kappa) |J| d\kappa q_\alpha^n - \int_{\Gamma_m} [Q_1^{N-n+1}(x(\kappa), \xi) + Q_2^{N-n}(x(\kappa), \xi)] N_\alpha(\kappa) |J| d\kappa u_\alpha^n \right] + u^{ff.N}(\xi), \quad (13)$$

where $U_1^{N-n+1} + U_2^{N-n}$ and $Q_1^{N-n+1} + Q_2^{N-n}$ are the closed form of scalar half-plane displacement and traction kernels, respectively (Panji 2013; Panji et al. 2014b). In addition, $u^{ff.N}$ and u^N are the free-field motion and displacement field in time step N , respectively. $N_\alpha(\kappa)$ is the quadratic shape functions in which κ is the local intrinsic coordinates of the elements. Also, u^n and q^n are displacement and traction vectors, respectively. In Eq. (13), the total number of boundary elements of the alluvial valley is presented by M . The portion of boundary to element ‘ m ’ is indicated by Γ_m , and J denotes the Jacobian of transformation. To calculate J , the following equation can be applied (Dominguez 1993):

$$J_i = \frac{\partial N_\alpha(\kappa)}{\partial \kappa} x_{i\alpha}, \quad (14)$$

4.3. Time-Stepping Algorithm

By discretizing the geometry boundary of the problem using three-node quadratic elements and forming the spatial integration of Eq. (13) for all BEs, the following matrix equation can be derived:

$$\sum_{n=1}^N H^{N-n+1} \{u^n\} = \sum_{n=1}^N G^{N-n+1} \{q^n\} + \{u^{ff.N}\}, \quad (15)$$

By integration over the boundary elements, the elements of H^{N-n+1} and G^{N-n+1} matrices can be obtained. The vectors of boundary nodal quantities at time-step n are indicated by $\{u^n\}$ and $\{q^n\}$. When the tractions on the boundary of the alluvial valley are absent, the term $G^{N-n+1} \{q^n\}$ should be considered equal to zero.

$$[A_1^1] \{X^N\} = [B_1^1] \{Y^N\} + \{R^N\} + \{u^{ff.N}\}, \quad (16)$$

in which:

$$\{R^N\} = \sum_{n=1}^{N-1} (G^{N-n+1} \{q^n\} - H^{N-n+1} \{u^n\}), \quad (17)$$

In Eq. (16), $\{X^N\}$ and $\{Y^N\}$ are the vectors including unknown and known variables, respectively, and $\{R^N\}$ includes the effects of past dynamic-history on the current time-node N . By solving Eq. (16), all boundary unknowns at each time-step can be calculated, and the displacements at any internal point ‘‘ m ’’ placed in the domain can be obtained.

5. Modeling

According to the sub-structuring process utilized in the half-plane time-domain BEM approach, based on Fig. 1, the alluvial valley must be divided into two parts, including a half-plane with a valley as the first part and a closed filled alluvium as the second part. The details of the modeling are presented in the following sections.

5.1. Part I: Hollow Valley

This part includes a half-plane medium with a surface valley subjected to seismic *SH*-waves. If the interface nodes of the valley connected to the surrounding domain are identified by subscript 12, the discretized BIE for this part at time step N can be written as follows:

$$H_{12}^1 u_{12}^N = G_{12}^1 q_{12}^N + R_{12}^N + u_{12}^{ff.N}, \quad (18)$$

In this equation, R_{12}^N is the past dynamic time history of the interface belonging to the first part and in the step N defined as follows:

$$R_{12}^N = \sum_{n=1}^{N-1} (G_{12}^{N-n+1} q_{12}^n - H_{12}^{N-n+1} u_{12}^n), \quad (19)$$

Also, u_{12}^N is the displacement and q_{12}^N is the traction field of interface Γ_{12} belonging to the first part, and $u_{12}^{ff.N}$ is the free-field motion of interface nodes.

5.2. Part II: A Closed Filled Alluvium

This part represents a closed filled solid medium as the alluvium. The interface nodes of this domain are identified by subscript 21, and the discretized BIE at the time step N can be written as follows:

$$H_{21}^2 u_{21}^N = G_{21}^2 q_{21}^N + R_{21}^N, \quad (20)$$

in which:

$$R_{21}^N = \sum_{n=1}^{N-1} (G_{21}^{N-n+1} q_{21}^n - H_{21}^{N-n+1} u_{21}^n), \quad (21)$$

where u_{21}^N and q_{21}^N are the displacement and traction fields of the interface Γ_{21} for the second part of the model, respectively. Also, R_{21}^N is the past dynamic time-history at time step N for the interface of the second part.

5.3. Assembling

In this step, the continuity conditions of the interface must be applied to solve the problem and obtain all the unknowns on the interface. Thus, the equilibrium conditions of displacement and the traction compatibility on the interface can be, respectively, presented as follows:

$$u_{12}^N = u_{21}^N, \quad (22)$$

and

$$\mu_1 q_{12}^N = -\mu_2 q_{21}^N, \quad (23)$$

where μ_1 and μ_2 are the shear modulus of the first and second parts of the model, respectively. Finally, by satisfying the mentioned conditions, the final matrix form of the assembled BIEs will be as follows:

$$\begin{bmatrix} H_{12}^1 & -1/\mu_1 G_{12}^1 \\ H_{21} & 1/\mu_2 G_{21}^1 \end{bmatrix} \begin{Bmatrix} u_{12}^N \\ q_{12}^N \end{Bmatrix} = \begin{Bmatrix} R_{12}^N \\ R_{21}^N \end{Bmatrix} + \begin{Bmatrix} u_{12}^{ff.N} \\ 0 \end{Bmatrix}, \quad (24)$$

By solving Eq. (24), all unknown values on the interface, such as displacements and tractions, can be obtained. Then, to calculate the displacements of the ground surface, the equations of the first part can be used by assuming $c(\xi) = 1.0$.

6. The DASBEM Program

This program is based on the half-plane boundary element method (BEM) and prepared for the dynamic analysis of plane scalar time domain problems. The name of DASBEM is taken from Dynamic Analysis of Structures by Boundary Element Method as well. The mentioned program is developed for seismic analysis of 2D semi-cylindrical alluvial valley located in an elastic half-plane. The flowchart and the details of this program are presented in the study of Panji, Mojtabazadeh-Hasanlouei, and Yasemi (2020).

7. Verification Study

The formulation was implemented in a general half-plane BEM code, previously called DASBEM (Panji et al. 2013a). To demonstrate the accuracy of this algorithm for the dynamic analysis of surface topographic features, a model of a semi-circular alluvial valley was prepared, established by the half-plane time-domain BEM. The mentioned alluvial valley was placed on the surface of a linear elastic half-plane subjected to incident *SH*-waves with the angles (θ) of 0° , 30° , 60° and 90° . The results were compared with the analytical results of Manoogian (1992) and Tsaor and Chang (2008a) presented for a single semi-circular alluvial valley. Figure 3 depicts the normalized displacement amplitude (NDA) of the ground surface. NDA is the ratio of the Fourier amplitude of the total ground surface motion obtained by BEM for a defined frequency to the Fourier amplitude of the incident motion for the mentioned defined frequency. In this example, the values of 0.5 and 1.0 are considered for dimensionless frequency (η) defined as ($\eta = \omega b / \pi c$). In this equation, ω is the angular frequency of the wave, b is the radius of the semi-circular alluvial valley and c is the shear-wave velocity. The value considered for impedance ratio (I) in this example is 0.3. The impedance ratio (I) is the stiffness ratio of the alluvium to the surrounding medium and explained as ($I = \rho_2 c_2 / \rho_1 c_1$), in which ρ_2 is the mass density and c_2 is the shear-wave velocity of the alluvium and ρ_1 and c_1 are the mass density and the shear-wave velocity of the surrounding medium, respectively. Therefore, the shear-wave velocity and the mass density of the alluvium are equal to 1080m.s^{-1} and 0.667ton.m^{-3} and the values of 2400m.s^{-1} and 1ton.m^{-3} are considered for the surrounding medium as well. Additionally, the predominant frequency and maximum amplitude of the *SH*-waves of the Ricker wavelet type are equal to 3 Hz and 0.001 m, respectively, and the time-shifting parameter is equal to 1.8 s. This problem is solved by 1000 time-steps with Δt of 0.007 s. The number of BEs considered for the semi-circular alluvial valley is equal to 127 elements. The numerical procedure is implemented in MATLAB (2019) programming software. By comparing the results with the solutions presented by Manoogian (1992) and Tsaor and Chang (2008a), a good agreement can be observed for the model of a single semi-circular alluvial valley. This verification example illustrated the good performance and applicability of this method for the dynamic analysis of advanced and complex engineering problems.

8. Application Examples

To study the behavior of a single alluvial valley located in an elastic half-plane subjected to seismic *SH*-waves, several key parameters are considered in the models and their effects are separately clarified. Based on Fig. 1, DR is the depth ratio of the alluvial valley and the values of 0.5, 1.0, 1.5 and 2.0 are considered in the modeling. Moreover, the incidence angles (θ) of 0° , 30° , 60° and 90° . The impedance ratios (I) of 0.1, 0.3 and 0.5 are applied, respectively. At first, to illustrate the reflection and diffraction of incidence waves for different scenarios, the results of time-domain are presented and then the results of frequency-domain are illustrated for specific cases to display the general pattern of motions and amplification values on the ground surface.

8.1. Time-Domain Responses

Utilizing the time-domain results is the only possible way to show the reflection and diffraction of the incidence waves. Thus, to illustrate the general pattern of responses and indicate the scattering of *SH*-

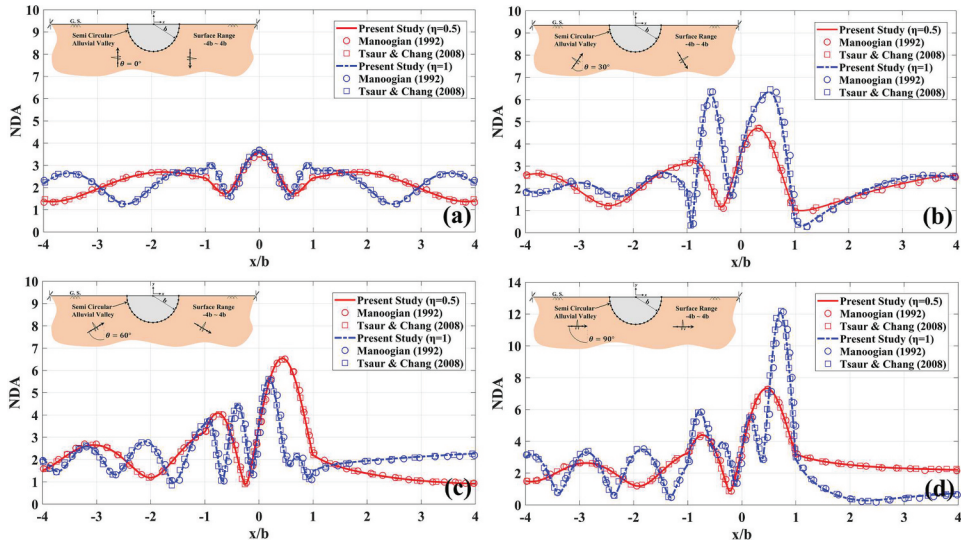


Figure 3. Normalized displacement amplitude of the ground surface versus x/b for the model of a single alluvial valley with the radius of b subjected to SH -waves and the incident angle of (a) $\theta = 0^\circ$, (b) $\theta = 30^\circ$, (c) $\theta = 60^\circ$ and (d) $\theta = 90^\circ$ for dimensionless frequencies (η) of 0.5 and 1.0.

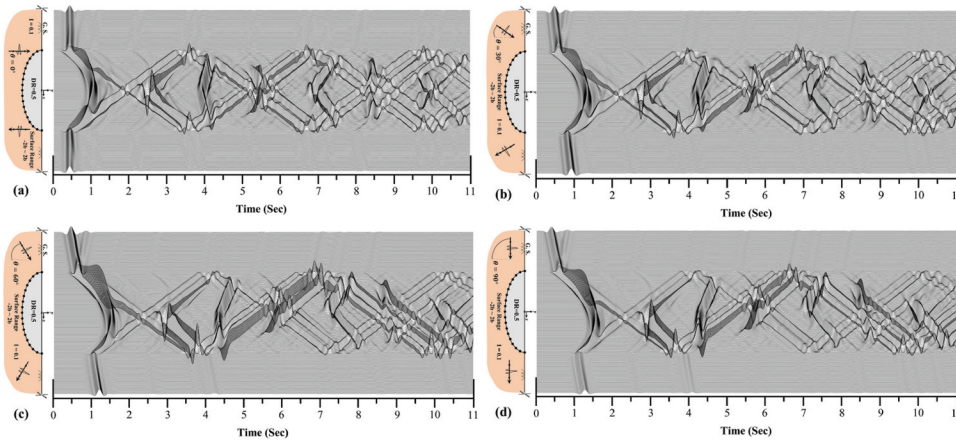


Figure 4. Synthetic seismograms of the ground surface and the procedure of SH -waves dispersion with time for the model of an alluvial valley with $I = 0.1$, $DR = 0.5$ and incident angle of (a) $\theta = 0^\circ$, (b) $\theta = 30^\circ$, (c) $\theta = 60^\circ$ and (d) $\theta = 90^\circ$.

waves in the time-domain, Figs. 4–15 are given for the model of an alluvial valley for different scenarios. The results are presented for the impedance ratios (I) of 0.1, 0.3, and 0.5 and the incidence angles (θ) of 0° , 30° , 60° and 90° , respectively. The factor of depth ratio (DR) is considered between 0.5 and 2.0 as well. According to the previous studies on the reflection and dispersion of incidence waves, when the incidence SH -waves are applied to the model, three phases of the waves are formed. The first part contains waves directly hitting the ground surface. The second phase is related to the waves encountering the valley’s boundary which a part of these waves is reflected and the other part is refracted into the alluvium. Moreover, the third phase contains crawler waves slipping on the boundary of the valley, reaching the ground surface and being reflected (Keller 1962).

Based on the above explanations, in the case of $I=0.1$, $DR = 0.5$ and $\theta = 0^\circ$, when the waves collide with the valley, some parts are directly reflected after hitting the valley’s boundary and the remaining part enters the medium of the alluvium. On the other hand, because of the low depth of the alluvium in

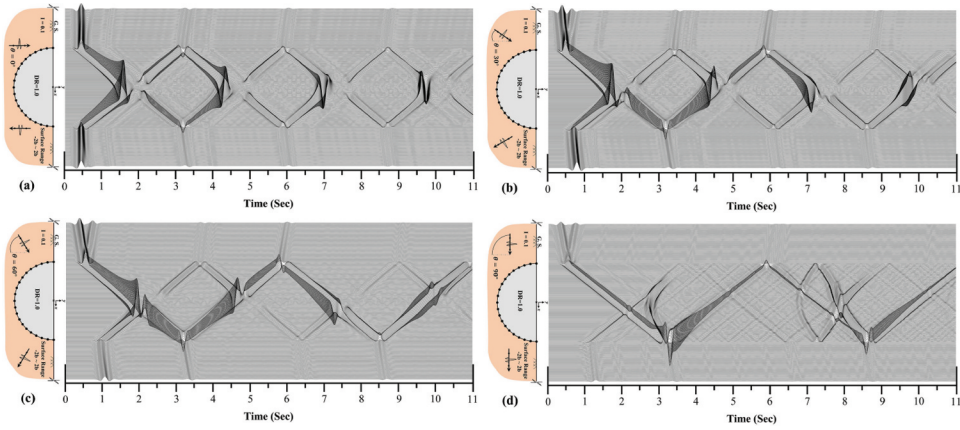


Figure 5. Synthetic seismograms of the ground surface and the procedure of *SH*-waves dispersion with time for the model of an alluvial valley with $l = 0.1$, $DR = 1.0$ and incident angle of (a) $\theta = 0^\circ$, (b) $\theta = 30^\circ$, (c) $\theta = 60^\circ$ and (d) $\theta = 90^\circ$.

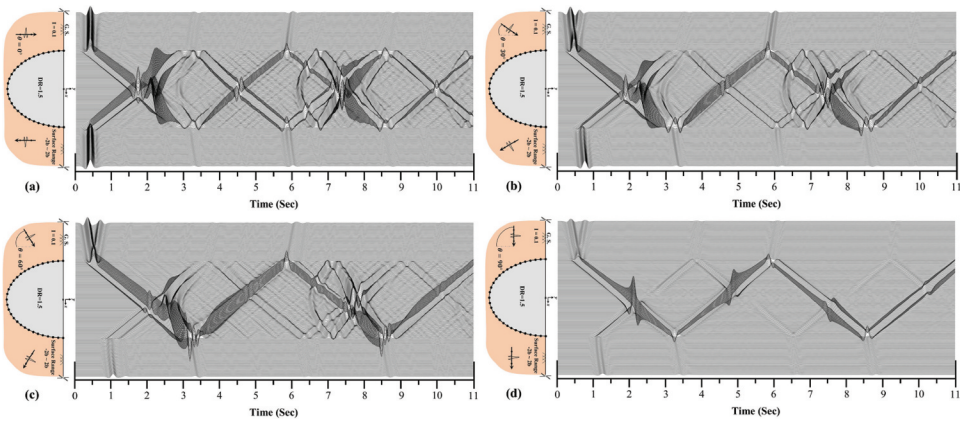


Figure 6. Synthetic seismograms of the ground surface and the procedure of *SH*-waves dispersion with time for the model of an alluvial valley with $l = 0.1$, $DR = 1.5$ and incident angle of (a) $\theta = 0^\circ$, (b) $\theta = 30^\circ$, (c) $\theta = 60^\circ$ and (d) $\theta = 90^\circ$.

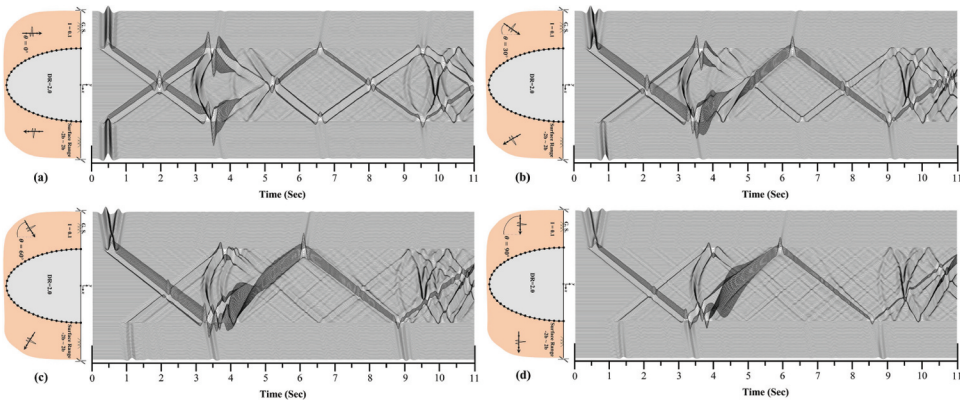


Figure 7. Synthetic seismograms of the ground surface and the procedure of *SH*-waves dispersion with time for the model of an alluvial valley with $l = 0.1$, $DR = 2.0$ and incident angle of (a) $\theta = 0^\circ$, (b) $\theta = 30^\circ$, (c) $\theta = 60^\circ$ and (d) $\theta = 90^\circ$.

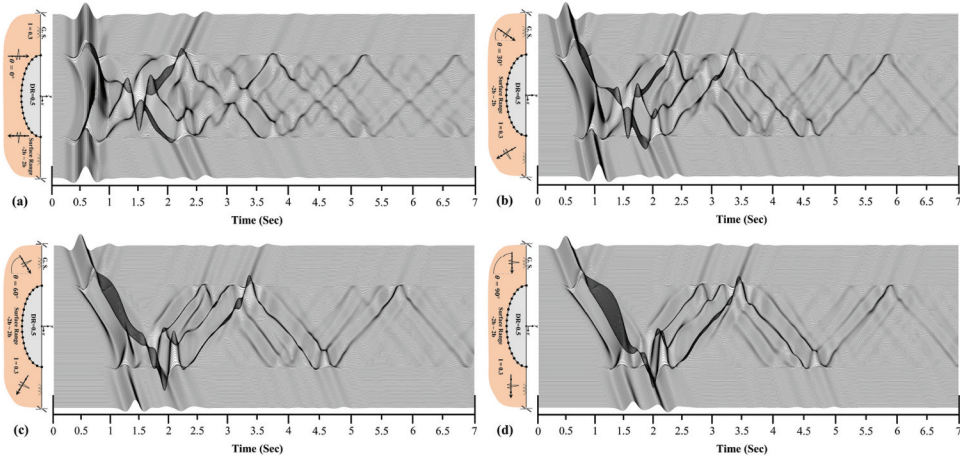


Figure 8. Synthetic seismograms of the ground surface and the procedure of *SH*-waves dispersion with time for the model of an alluvial valley with $l = 0.3$, $DR = 0.5$ and incident angle of (a) $\theta = 0^\circ$, (b) $\theta = 30^\circ$, (c) $\theta = 60^\circ$ and (d) $\theta = 90^\circ$.

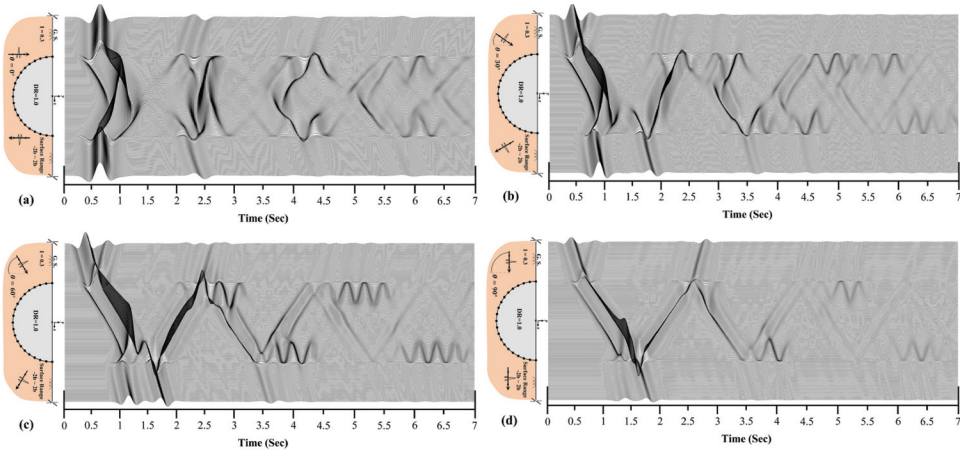


Figure 9. Synthetic seismograms of the ground surface and the procedure of *SH*-waves dispersion with time for the model of an alluvial valley with $l = 0.3$, $DR = 1.0$ and incident angle of (a) $\theta = 0^\circ$, (b) $\theta = 30^\circ$, (c) $\theta = 60^\circ$ and (d) $\theta = 90^\circ$.

lower values of DR , the crawler waves are quickly slipped on the valley's boundary and reach the surface from the sides of the valley and are then reflected inside the medium of alluvium. Afterwards, the boundary of the valley acts like a mirror because of the very high stiffness of the outside medium compared to the stiffness of alluvium. Thus, the effect of wave trapping occurred inside the valley, resulting in high amplitude of displacements on the ground surface. Over time, this effect will increase the complexity of the results as well. For $DR = 1.0$, the regular form of the valley helps the waves to reflect uniformly. Therefore, this effect creates uniform paths of the trapped waves and the highest amplitudes appear in the middle of the alluvium where the paths of reflected waves encounter each other and gradually reduce the amplitudes over time. In $I=0.1$, $DR = 1.5$ and $\theta = 0^\circ$, the higher volume of the refracted waves enters the alluvium, and the higher volume of crawler waves is slipped on the boundary of valley. In this case, the first collision of the wave paths occurs with more intensity. Also, the greater depth of the valley increases the arrival time and amplitude of the waves. Therefore, when $DR = 1.5b$, the complexity of the result is lower than the case of $DR = 0.5$, but the collision of the wave paths occurs with a higher intensity for higher DR s. For $I=0.1$, $DR = 2.0$ and $\theta = 0^\circ$, because of the larger volume of influential waves and the longer paths traversed by waves inside the alluvium, the

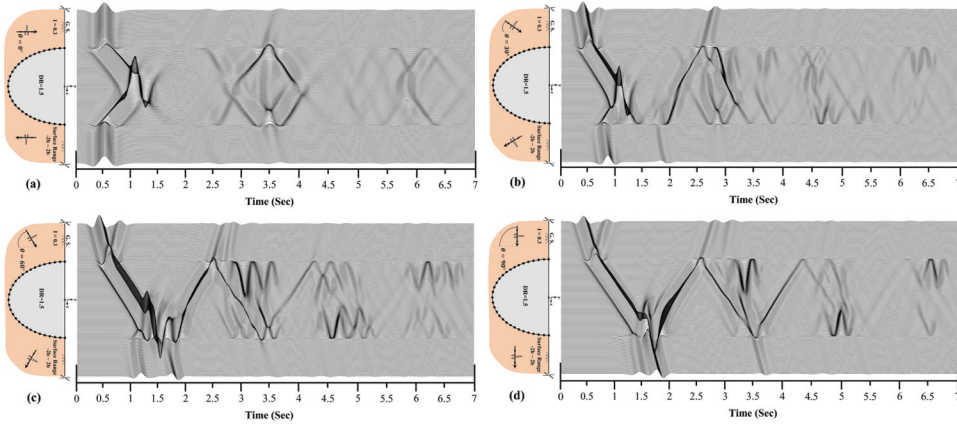


Figure 10. Synthetic seismograms of the ground surface and the procedure of SH -waves dispersion with time for the model of an alluvial valley with $I = 0.3$, $DR = 1.5$ and incident angle of (a) $\theta = 0^\circ$, (b) $\theta = 30^\circ$, (c) $\theta = 60^\circ$ and (d) $\theta = 90^\circ$.

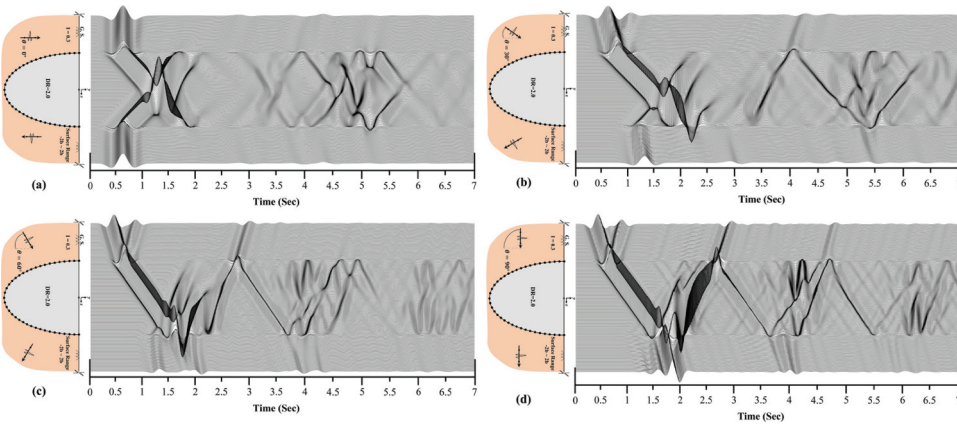


Figure 11. Synthetic seismograms of the ground surface and the procedure of SH -waves dispersion with time for the model of an alluvial valley with $I = 0.3$, $DR = 2.0$ and incident angle of (a) $\theta = 0^\circ$, (b) $\theta = 30^\circ$, (c) $\theta = 60^\circ$ and (d) $\theta = 90^\circ$.

complexity of the result is greatly decreased, while the amplitudes are very high. In fact, longer paths and higher amplitudes help the waves stay in their paths, even when they collide with each other. The main complexity is formed for the first time when they hit the boundary of the valley after entering the alluvium. Inclination of the wave front to $\theta = 30^\circ$ eliminates the symmetry of the results in all cases. When $I=0.1$ and $\theta = 30^\circ$, the highest amplitudes emerge in the paths of waves parallel to the wave front and the incidence waves follow the same entrance paths into the alluvium. This effect is much clearer when the angle of incidence waves is closer to the horizon.

When $I=0.3$, the stiffness of the alluvium increases and leads to decrease the waves amplitude and lower displacements of the ground surface. Therefore, the results show a lower level of complexity compared to the results of $I=0.1$. Nevertheless, in the cases of $I=0.3$, the most vibrations are achieved in the lowest DR value which is because of small medium of alluvium for wave reflections. Like previous cases, increasing the DR value results in less complexity but higher amplitudes of responses. On the other hand, when the stiffness of alluvium is very low ($I=0.1$), by applying the oblique wave front to the models, the alluvium acts like a barrier and reduces the amplitudes of the motions on the opposite side to the wave front called the “shadow zone” (Trifunac 1973). In fact, the lower stiffness of the alluvium increases the effect of the shadow zone and this phenomenon is weaker for the models with higher impedance ratios. Thus, the results of $I=0.1$ cases

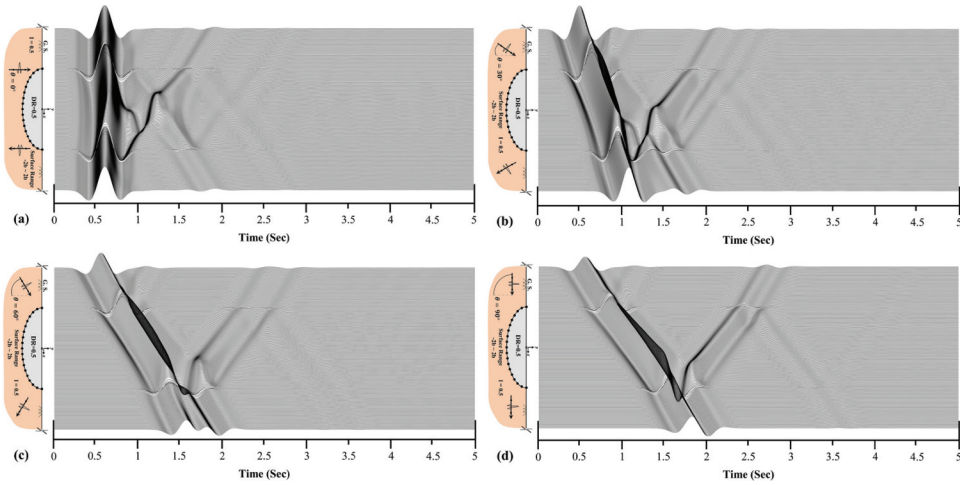


Figure 12. Synthetic seismograms of the ground surface and the procedure of *SH*-waves dispersion with time for the model of an alluvial valley with $I = 0.5$, $DR = 0.5$ and incident angle of (a) $\theta = 0^\circ$, (b) $\theta = 30^\circ$, (c) $\theta = 60^\circ$ and (d) $\theta = 90^\circ$.

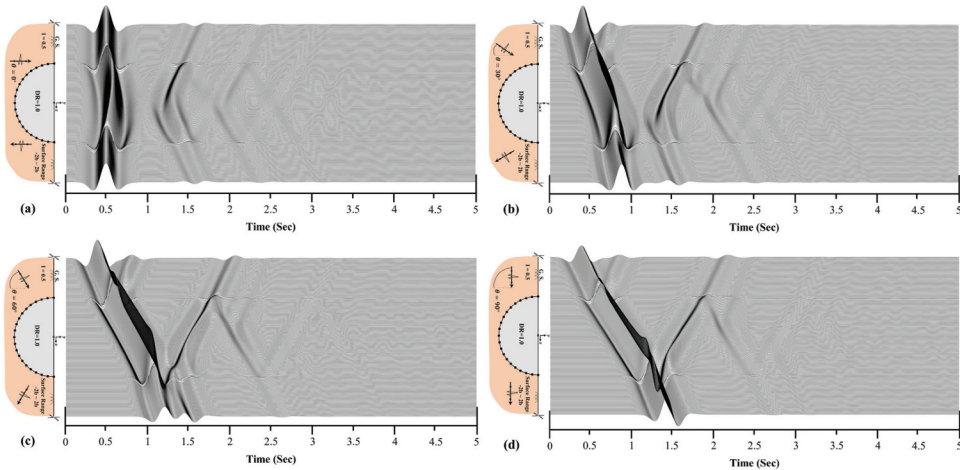


Figure 13. Synthetic seismograms of the ground surface and the procedure of *SH*-waves dispersion with time for the model of an alluvial valley with $I = 0.5$, $DR = 1.0$ and incident angle of (a) $\theta = 0^\circ$, (b) $\theta = 30^\circ$, (c) $\theta = 60^\circ$ and (d) $\theta = 90^\circ$.

demonstrate the strongest effect on the attenuation and prevention of the wave passage which is clearer in higher DRs. Also, the results of $I=0.5$ for different DR values and incidence angles show that when the stiffness of the alluvium is equal to half compared to the stiffness of outside medium, the responses of the ground surface are closely similar to the free-field motions. Thus, the amount of complexity and amplitudes decreases and the required time for wave reflection and refraction is reduced as well. An essential point in the results is the role of alluvium’s stiffness in the required time to reach convergence in the responses. The lower stiffness of alluvium leads to a more flexible behavior and a higher volume of trapped waves inside the alluvium. Thus, more displacements will occur on the ground surface, and the waves leave the closed medium of alluvium more slowly. Therefore, more time will be needed to reach convergence and calmness in the results. However, by increasing the stiffness of the alluvium, its behavior becomes more similar to the outside medium of the valleys and the waves leave the model faster than the previous cases.

Figures 16–19 are presented to show the amplitude of incidence *SH*-waves against the time in the presence of a single alluvial valley with depth ratios (DR) of 0.5, 1.0, 1.5 and 2.0 and impedance ratio (I) of 0.3 for the

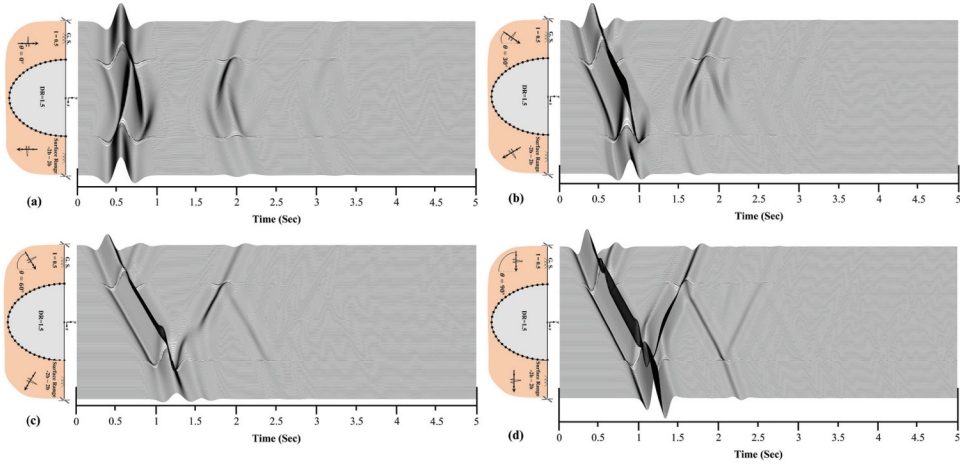


Figure 14. Synthetic seismograms of the ground surface and the procedure of SH -waves dispersion with time for the model of an alluvial valley with $l = 0.5$, $DR = 1.5$ and incident angle of (a) $\theta = 0^\circ$, (b) $\theta = 30^\circ$, (c) $\theta = 60^\circ$ and (d) $\theta = 90^\circ$.

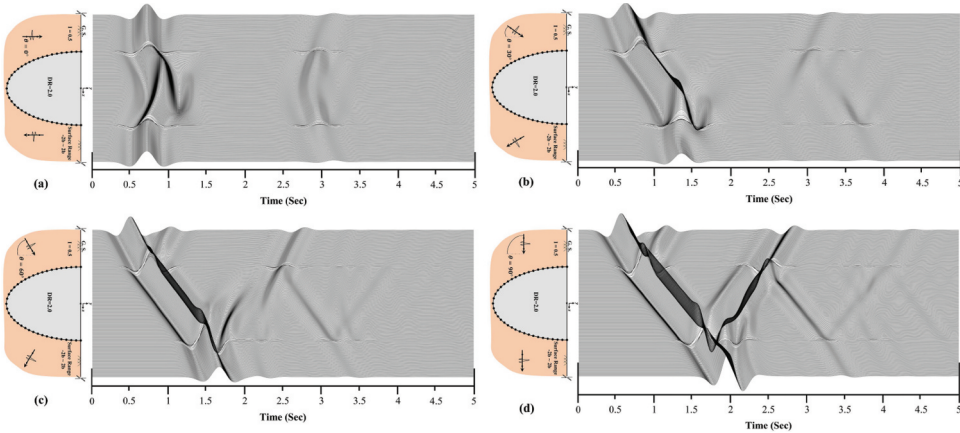


Figure 15. Synthetic seismograms of the ground surface and the procedure of SH -waves dispersion with time for the model of an alluvial valley with $l = 0.5$, $DR = 2.0$ and incident angle of (a) $\theta = 0^\circ$, (b) $\theta = 30^\circ$, (c) $\theta = 60^\circ$ and (d) $\theta = 90^\circ$.

incidence angles (θ) of 0° , 30° , 60° , and 90° . For this purpose, three reference stations are considered on the surface where (1) and (3) are located at the edges and (2) is placed at the center of the alluvial valley as well. The results are compared beside the response of free-field to see the difference of wave propagation in the time-domain. The amplitude is the ratio of ground surface displacement to the maximum acceleration of applied waves. As can be seen, when the angle of incidence waves (θ) is equal to 0° , the diagrams of stations (1) and (3) are coincident. But, by inclination of the wave front, the difference between diagrams is noticeable. As depicted in the figures, the maximum amplitude is occurred in $DR = 1.5$ and angle (θ) of 0° with amplitude of 8. In this model, the non-uniformity of alluvial valley section helped the waves to concentrated exactly on the position of station (2).

8.2. Amplification Patterns

Presenting the results of frequency-domain is the only possible way to demonstrate the general pattern of ground surface displacements in the presence of an alluvial valley and show its behavior subjected to

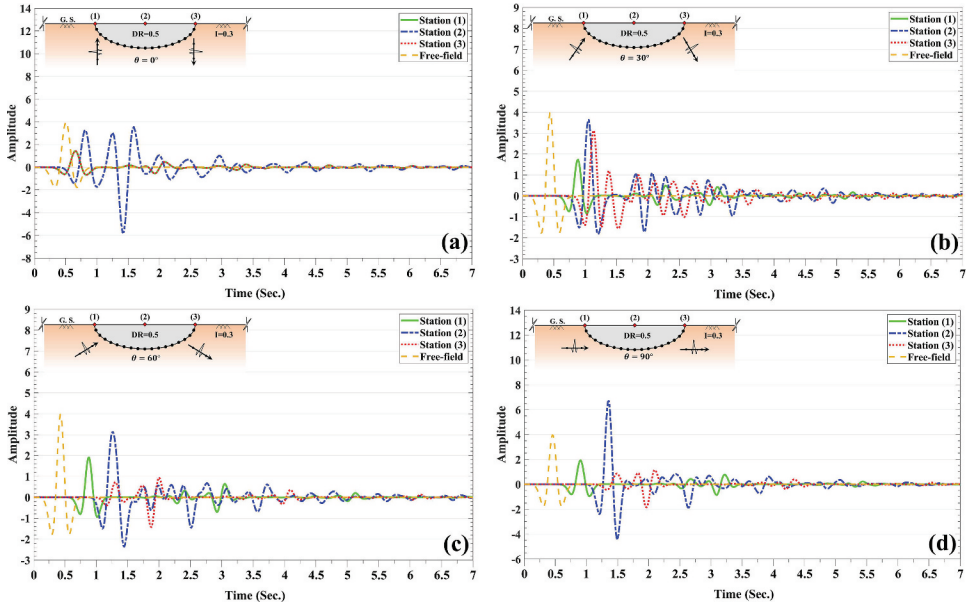


Figure 16. The amplitude of scattered waves on the ground surface for the model of an alluvial valley with $I = 0.3$, $DR = 0.5$ and incident angle of (a) $\theta = 0^\circ$, (b) $\theta = 30^\circ$, (c) $\theta = 60^\circ$ and (d) $\theta = 90^\circ$.

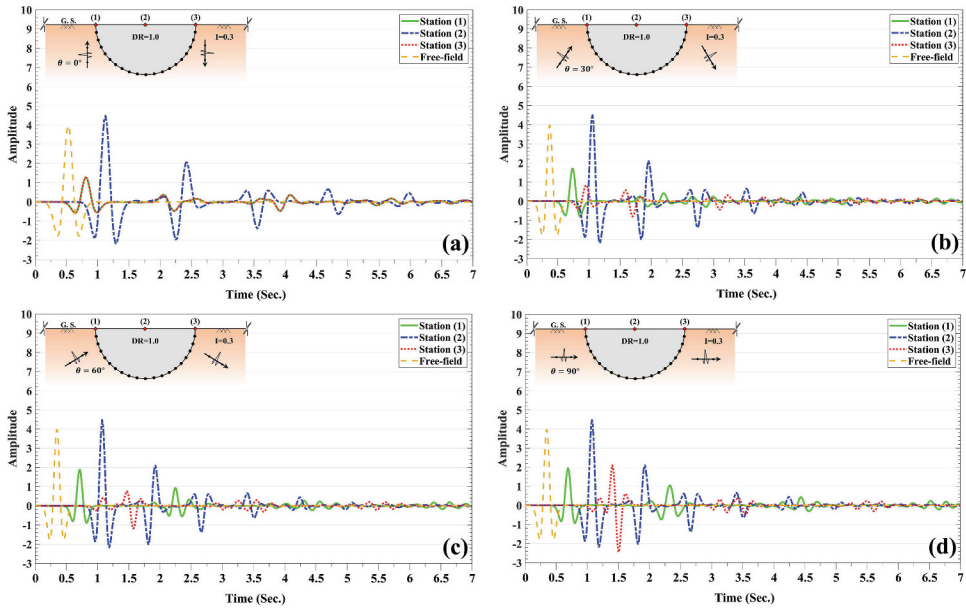


Figure 17. The amplitude of scattered waves on the ground surface for the model of an alluvial valley with $I = 0.3$, $DR = 1.0$ and incident angle of (a) $\theta = 0^\circ$, (b) $\theta = 30^\circ$, (c) $\theta = 60^\circ$ and (d) $\theta = 90^\circ$.

seismic waves. Therefore, Figs. 20–23 are provided for this purpose. In the presented results, the factor of amplification is defined as the ratio of surface response amplitude to free-field motion. In this section, the results of $I=0.3$ are presented for various angles of incidence waves and depth ratios. The range of amplification color-bar is set between 0 and 10 and the dimensionless frequency is considered between 0.25 and 3 in all of the responses. Also, the surface range is closed between $-3b$ to $3b$. Like the

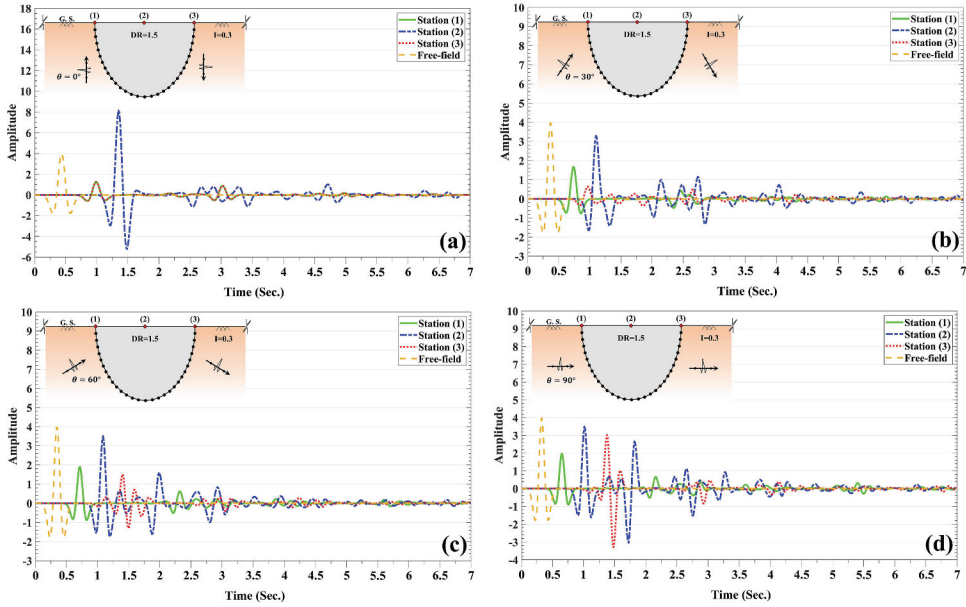


Figure 18. The amplitude of scattered waves on the ground surface for the model of an alluvial valley with $l = 0.3$, $DR = 1.5$ and incident angle of (a) $\theta = 0^\circ$, (b) $\theta = 30^\circ$, (c) $\theta = 60^\circ$ and (d) $\theta = 90^\circ$.

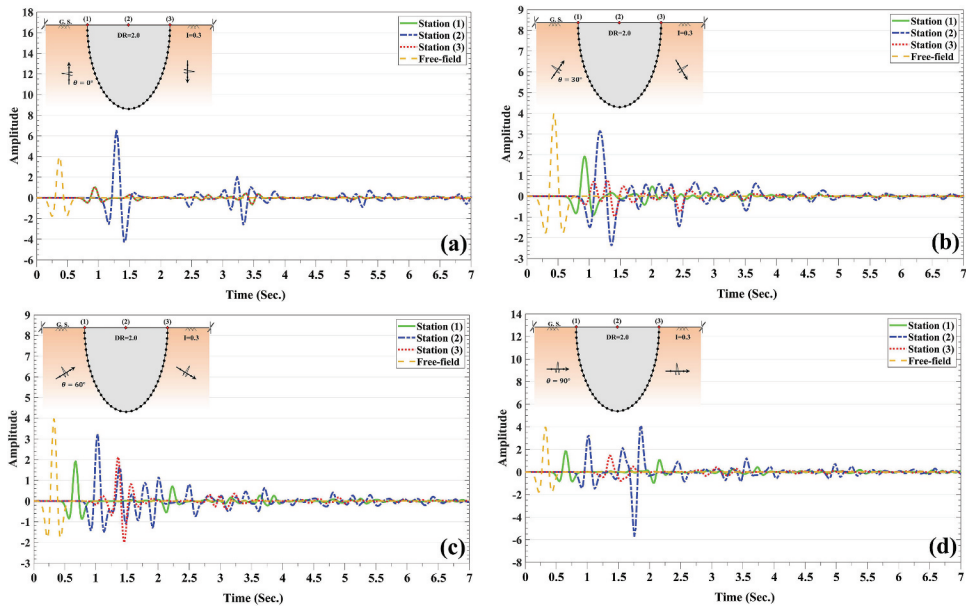


Figure 19. The amplitude of scattered waves on the ground surface for the model of an alluvial valley with $l = 0.3$, $DR = 2.0$ and incident angle of (a) $\theta = 0^\circ$, (b) $\theta = 30^\circ$, (c) $\theta = 60^\circ$ and (d) $\theta = 90^\circ$.

previous section, the angles of incidence waves (θ) are considered as 0° , 30° , 60° , and 90° and the factor of DR is 0.5 to 2.0. Based on the responses, when the angle of incidence waves is equal to 0° , all the results are symmetric. It is clear that the vibrations of diagrams change in the presence of an alluvial valley and higher amplifications are achieved in its location. In fact, due to the softer content of

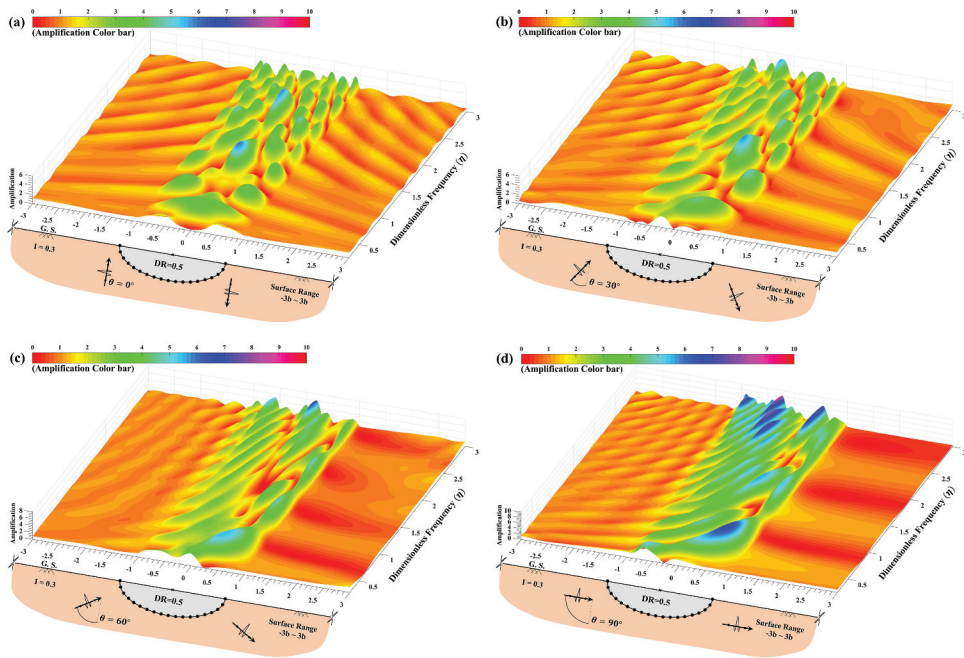


Figure 20. 3D amplification of the ground surface versus different dimensionless frequencies for the model of an alluvial valley subjected to *SH*-waves with $I = 0.3$, $DR = 0.5$ and the incident angle of (a) $\theta = 0^\circ$, (b) $\theta = 30^\circ$, (c) $\theta = 60^\circ$ and (d) $\theta = 90^\circ$.

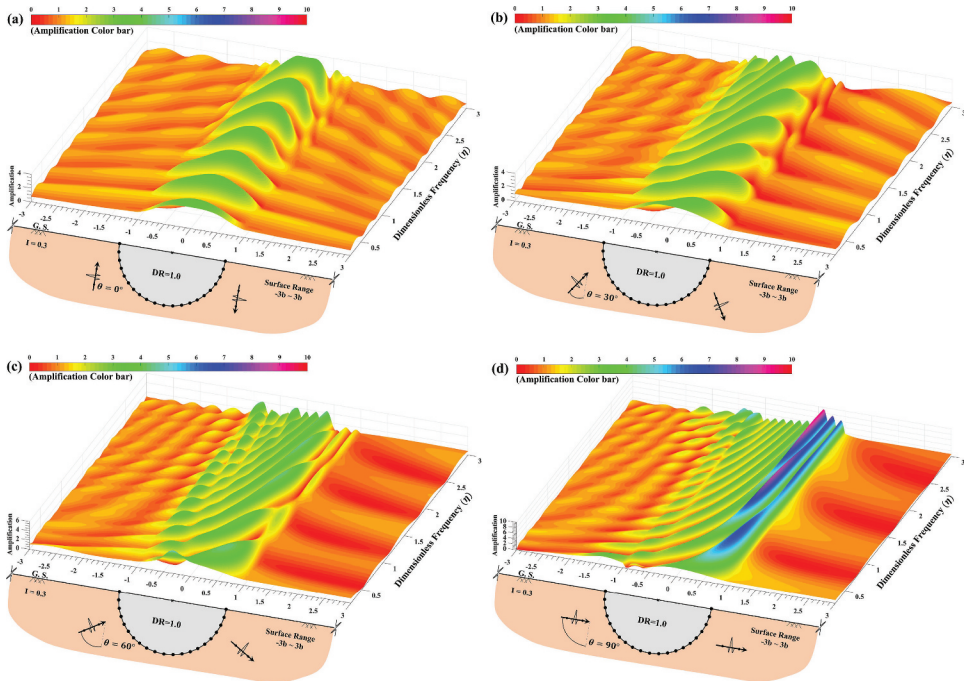


Figure 21. 3D amplification of the ground surface versus different dimensionless frequencies for the model of an alluvial valley subjected to *SH*-waves with $I = 0.3$, $DR = 1.0$ and the incident angle of (a) $\theta = 0^\circ$, (b) $\theta = 30^\circ$, (c) $\theta = 60^\circ$ and (d) $\theta = 90^\circ$.

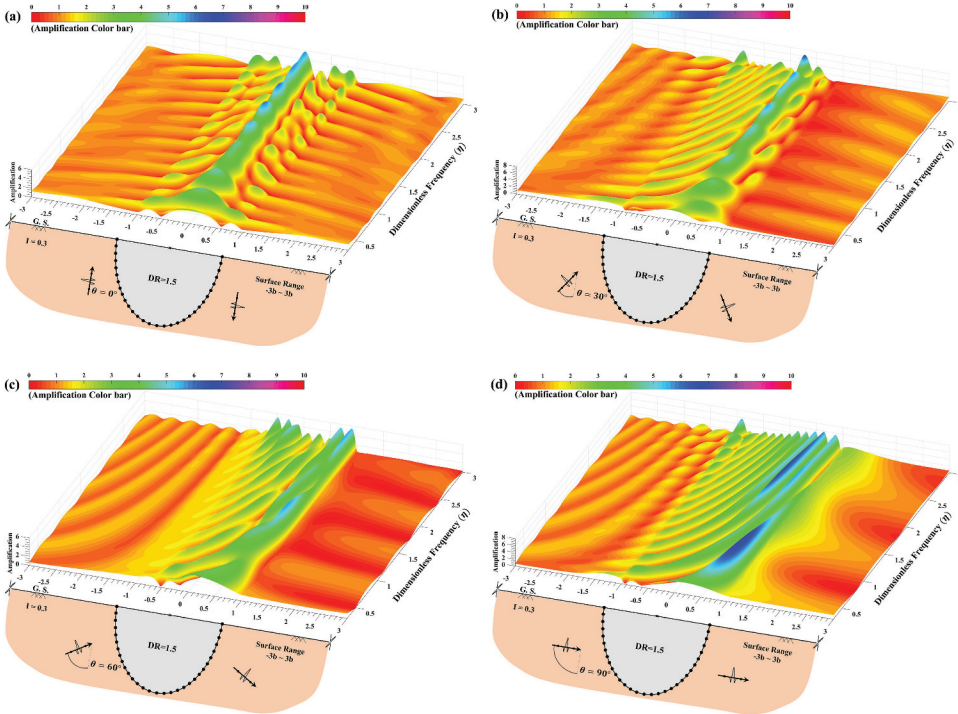


Figure 22. 3D amplification of the ground surface versus different dimensionless frequencies for the model of an alluvial valley subjected to SH -waves with $I = 0.3$, $DR = 1.5$ and the incident angle of (a) $\theta = 0^\circ$, (b) $\theta = 30^\circ$, (c) $\theta = 60^\circ$ and (d) $\theta = 90^\circ$.

alluvium compared to the surrounding medium, applying seismic waves to the model increases the amplitudes of displacements on the ground surface. Therefore, the amount of amplifications in the location of alluvial valley will be much higher than the surrounding zones. Based on these explanations, when DR is equal to 0.5, amplifications appear as separated vibrations on the 3D diagram. This form of responses is because of the intermittent reflections of the waves inside the small medium of alluvium. When $I=0.3$, the soft content of alluvium causes the waves to be trapped inside the alluvium. In this position, because of the higher stiffness of the outside medium compared to alluvium, the boundary of the valley acts like a reflective surface and does not allow the waves to quickly leave the alluvium. This effect provides the condition of multiple reflections. Thus, when these reflected waves collide each other, hit the valley's boundary or hit the ground surface, the final result will appear as a vibration on the diagram. By reducing DR , the reflections should occur in shorter paths. Thus, the complexity of the results will be increased by the same amount.

By inclining the waves front to 30° , the symmetry of results is eliminated. Comparing the results of $\theta = 0^\circ$ and $\theta = 30^\circ$ for $DR = 0.5$ reveals that the differences are few, but unlike the case of $\theta = 0^\circ$, the vibrations and amplification paths in the diagram of $\theta = 30^\circ$ slightly follow each other. This effect is much stronger for the cases of $\theta = 60^\circ$ and $\theta = 90^\circ$ indicating that by the inclination of the wave front to reach the horizon, the incidence waves move on longer paths. Therefore, the amplifications become higher and the amount of intermittent reflections inside the alluvium becomes lower. Also, by applying the wave front in the horizontal angle, the effect of shadow zone becomes stronger because of more attenuations of the waves during their passage from the inside of the alluvium. For the cases of $DR = 1.0$, the paths of amplifications are fully harmonious and uniform which is because of the regular shape of valley. It is evident that the highest amplifications occur in the case of $DR = 1.0$ and $\theta = 90^\circ$ with a value of about 8 times compared to the free-field. Furthermore, the phenomenon of shadow zone is quite clear in this case.

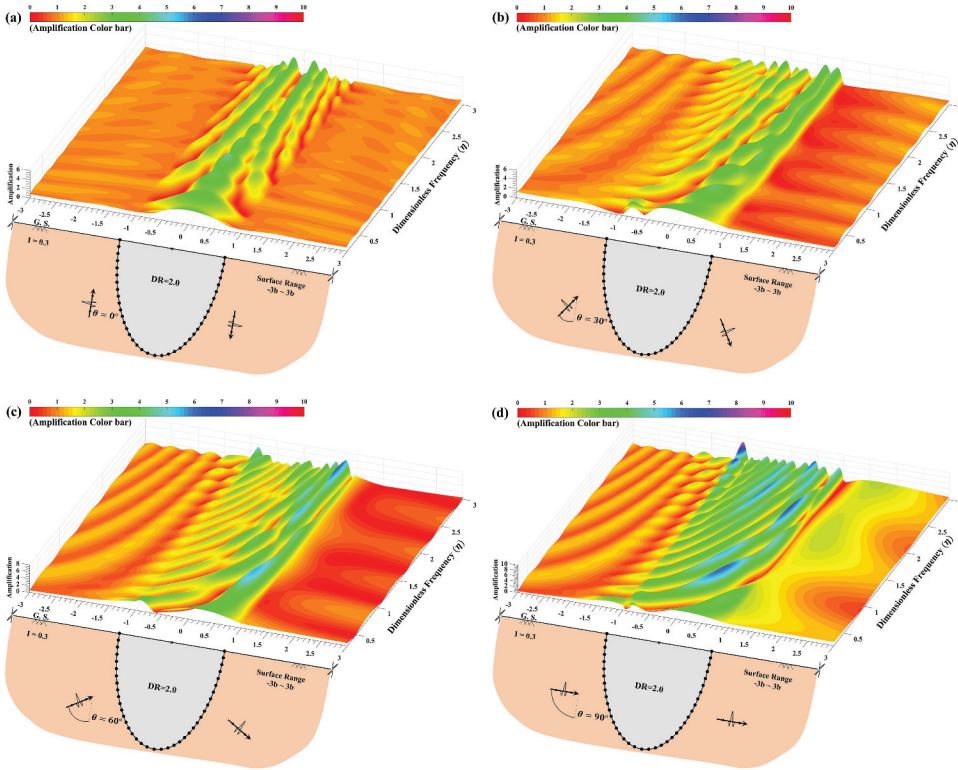


Figure 23. 3D amplification of the ground surface versus different dimensionless frequencies for the model of an alluvial valley subjected to SH -waves with $I = 0.3$, $DR = 2.0$ and the incident angle of (a) $\theta = 0^\circ$, (b) $\theta = 30^\circ$, (c) $\theta = 60^\circ$ and (d) $\theta = 90^\circ$.

When $DR = 1.5$ and $\theta = 0^\circ$, maximum amplifications occur in the middle of the alluvium. In fact, due to the specific shape of the alluvial valley, the collisions of waves occur in a single path in the middle of the alluvium, leading to higher amplifications in the middle of the valley. Nevertheless, in the case of $DR = 2.0$, multiple paths are emerged. On the other hand, by comparing the results of lower DR values with $DR = 2.0$ and for the incidence angle of $\theta = 90^\circ$, it is understood that when the depth ratio of the alluvial valley is higher than 1.5, a massive volume of waves can enter the medium of alluvium. Therefore, the content of alluvium cannot attenuate the waves and the effect of the shadow zone will be much weaker than lower DR values. Moreover, increasing the DR value beyond 1.0 cannot increase maximum amplifications.

9. Conclusions

The response of the ground surface in the presence of an alluvial valley was presented in time and frequency domains. The model was placed in a linear elastic half-plane subjected to incident out-of-plane SH -waves. Modeling was performed by developing a predefined approach known as half-plane time-domain BEM for an alluvial valley site. One of the abilities of the proposed method was to concentrate the meshes only around the interface. By applying this method to each part of the model, including valley and alluvium, and assembling their formulations, the influence coefficients of the matrices were obtained. Therefore, the boundary values of displacement fields could be determined. After presenting the formulation, a verification example was explored for a semi-circular alluvial valley and the results were compared with those presented in the technical literature. The results illustrated the acceptable performance of the introduced method and its high accuracy for the seismic analysis of intricate engineering problems. Next, an advanced numerical study was conducted to demonstrate the ground surface

responses in the presence of a semi-cylindrical alluvial valley with different impedances and depth ratios as synthetic seismograms under obliquely incident *SH*-waves. In the final section, the amplification patterns were illustrated for the impedance ratio of 0.3 and various depth ratios as 3D diagrams in the frequency-domain. The most important results of this study can be summarized as follows:

(a) The lower impedance ratio leads to more flexible behavior of the alluvium and a higher volume of trapped waves. Thus, more displacements occur on the ground surface and the waves leave the alluvium more slowly. For $I=0.1$ and oblique wave front, the highest amplitudes emerge in the paths of waves parallel to the wave front and follow the same entrance paths into the alluvium. This effect is much clearer when the angle of incidence waves is closer to the horizon.

(b) When the stiffness of alluvium is very low, the alluvium acts like a barrier to oblique incidence waves and reduces the amplitudes of the motions on the opposite side of the wave front. This effect, however, is weaker for higher impedance ratios.

(c) For $I=0.5$, the responses of the ground surface are similar to the free-field motions. Thus, the volume of complexity and amplitudes decreases, the required convergence time of the results is reduced.

(d) Most vibrations are achieved in the results of $DR = 0.5$ because of the small limited medium of alluvium and intermittent reflections of the waves. In addition, for $DR = 1.0$, the regular form of the valley assists the waves in creating the uniform paths of the trapped waves and the highest amplitudes appear in the middle of the alluvium. By increasing the depth ratio of the valley, the complexity of the result is decreased, but the amplitudes are increased. Moreover, the highest amplifications occur in the case of $DR = 1.0$ and $\theta = 90^\circ$ with the value of about 8 times compared to free-field. In fact, by inclining the wave front to reach the horizon, amplifications become higher and the amount of intermittent reflections inside the alluvium becomes lower. When the angle of wave front is $\theta = 90^\circ$, the effect of the shadow zone becomes stronger because of the higher attenuations of the waves during their passage from inside the alluvium.

(e) When $DR = 1.5$ and $\theta = 0^\circ$, the maximum amplifications occur in the middle of the alluvium. Nevertheless, in the case of $DR = 2.0$, multiple paths emerge. When the depth ratio of the alluvial valley is higher than 1.5, a massive volume of waves is able to enter the alluvium. However, the alluvium cannot diminish the waves and the effect of the shadow zone is much weaker than the lower DR values. Moreover, increasing the DR value after 1.0 cannot increase maximum amplifications.

Note

1. Dynamic Analysis of Structures by the Boundary Element Method.

ORCID

Mehdi Panji  <http://orcid.org/0000-0002-3240-7775>

Saeed Mojtabazadeh-Hasanlouei  <http://orcid.org/0000-0001-8508-4837>

References

- Aki, K. 1988. Local site effects and strong ground motion. Proceedings of the special conference on earthquake engineering and soil dynamics 2. Park City, UT: American Society of Civil Engineers.
- Aki, K. 1993. Local site effects on weak and strong ground motion. *Tectonophysics* 218 (1–3): 93–111. doi: 10.1016/0040-1951(93)90262-I.
- Aki, K., and K. L. Larner. 1970. Surface motion of a layered medium having an irregular interface due to incident plane *SH* waves. *Journal of Geophysical Research* 75 (5): 933–54. doi: 10.1029/JB075i005p00933.
- Ausilio, E., E. Conte, and G. Dente. 2008. Seismic response of alluvial valleys to *SH*-waves. *Seismic Engineering Conference AIP Conference Proceedings* 1020: 199–206.
- Ba, Z., and J. Liang. 2017. Dynamic response analysis of periodic alluvial valleys under incident plane *SH*-waves. *Journal of Earthquake Engineering* 21 (4): 531–50. doi: 10.1080/13632469.2016.1178192.
- Ba, Z., and X. Yin. 2016. Wave scattering of complex local site in a layered half-space by using a multidomain IBEM: Incident plane *SH* waves. *Geophysical Journal International* 205 (3): 1382–405. doi: 10.1093/gji/ggw090.

- Bard, P. Y., and M. Bouchon. 1980a. The seismic response of sediment-filled valleys, Part 1. The case of incident *SH*-waves. *Bulletin of the Seismological Society of America* 70: 1263–86.
- Bard, P. Y., and M. Bouchon. 1980b. The seismic response of sediment-filled valleys, Part 2. The case of incident *P* and *SV*-waves. *Bulletin of the Seismological Society of America* 70: 1921–41.
- Bielak, J., J. Xu, and O. Ghattas. 1999. Earthquake ground motion and structural response in alluvial valleys. *Journal of Geotechnical and Geoenvironmental Engineering*, ASCE. 125 (5): 413–23. doi: [10.1061/\(ASCE\)1090-0241\(1999\)125:5\(413\)](https://doi.org/10.1061/(ASCE)1090-0241(1999)125:5(413)).
- Boore, D. M. 1972. A note on the effect of simple topography on seismic *SH*-waves. *Bulletin of the Seismological Society of America* 62: 275–84.
- Bouchon, M. 1973. Effect of topography on surface motion. *Bulletin of the Seismological Society of America* 63 (3): 715–32.
- Brebbia, C. A., and J. Dominguez. 1989. *Boundary elements, an introductory course*. Southampton, Boston: Comp Mech Pub.
- Chang, K. H., D. H. Tsaur, and J. H. Wang. 2013. Scattering of *SH* waves by a circular sectorial canyon. *Geophysical Journal International* 195: 532–43. doi: [10.1093/gji/ggt236](https://doi.org/10.1093/gji/ggt236).
- Chang, K. H., D. H. Tsaur, and J. H. Wang. 2015. Response of a shallow asymmetric V-shaped canyon to anti-plane elastic waves. *Proceedings. Mathematical, Physical, and Engineering Sciences* 471: 2174:20140215. doi: [10.1098/rspa.2014.0215](https://doi.org/10.1098/rspa.2014.0215).
- Davis, L. L., and L. R. West. 1973. Observed effects of topography on ground motion. *Bulletin of the Seismological Society of America* 63 (1): 283–98.
- Dominguez, J. 1993. *Boundary elements in dynamics*. Southampton, Boston: Comp Mech Pub.
- Dravinski, M. 1983. Amplification of *P*, *SV*, and *Rayleigh*-waves by two alluvial valleys. *International Journal of Soil Dynamics and Earthquake Engineering* 2 (2): 66–77.
- Esteva, L. 1977. Microzoning: Models and reality. Proceedings of 6th World Conference on Earthquake Engineering, New Delhi.
- Faik-Kara, H., and M. D. Trifunac. 2013. A note on plane-wave approximation. *Soil Dynamics and Earthquake Engineering* 51: 9–13. doi: [10.1016/j.soildyn.2013.04.003](https://doi.org/10.1016/j.soildyn.2013.04.003).
- Faik-Kara, H., and M. D. Trifunac. 2014. Two-dimensional earthquake vibrations in sedimentary basins – *SH* waves. *Soil Dynamics and Earthquake Engineering* 63: 69–82. doi: [10.1016/j.soildyn.2014.03.010](https://doi.org/10.1016/j.soildyn.2014.03.010).
- Fishman, K. L., and S. Ahmad. 1995. Seismic response for alluvial valleys subjected to *SH*, *P* and *SV*-waves. *Soil Dynamics and Earthquake Engineering* 14 (4): 249–58. doi: [10.1016/0267-7261\(94\)00049-M](https://doi.org/10.1016/0267-7261(94)00049-M).
- Frankel, A., and J. A. Vidale. 1992. Three-dimensional simulation of seismic waves in the Santa Clara Valley, California, from a Loma Prieta Aftershock. *Bulletin of the Seismological Society of America* 82: 2045–74.
- Gao, F., C. Zhao, and J. Dong. 2006. An analytical solution for three-dimensional diffraction of plane *P*-waves by a hemispherical alluvial valley with saturated soil deposits. *Acta Mechanica Solida Sinica* 19 (2): 141–51. doi: [10.1007/s10338-006-0617-5](https://doi.org/10.1007/s10338-006-0617-5).
- Garcia-Sanchez, F., and C. Zhang. 2007. A comparative study of three BEM for transient dynamic crack analysis of 2-D anisotropic solids. *Computational Mechanics* 40 (4): 753–769.
- Gatmiri, B., and C. Arson. 2008b. Seismic site effects by an optimized 2D BE/FE method II. Quantification of site effects in two-dimensional sedimentary valleys. *Soil Dynamics and Earthquake Engineering* 28 (8): 646–61. doi: [10.1016/j.soildyn.2007.09.002](https://doi.org/10.1016/j.soildyn.2007.09.002).
- Gatmiri, B., C. Arson, and K. V. Nguyen. 2008a. Seismic site effects by an optimized 2D BE/FE method I. Theory, numerical optimization and application to topographical irregularities. *Soil Dynamics and Earthquake Engineering* 28 (8): 632–45. doi: [10.1016/j.soildyn.2007.09.001](https://doi.org/10.1016/j.soildyn.2007.09.001).
- Gil-Zepeda, S. A., J. C. Montalvo-Arrieta, R. Vai, and F. J. Sánchez-Sesma. 2003. A hybrid indirect boundary element-discrete wave number method applied to simulate the seismic response of stratified alluvial valleys. *Soil Dynamics and Earthquake Engineering* 23 (1): 77–86. doi: [10.1016/S0267-7261\(02\)00092-1](https://doi.org/10.1016/S0267-7261(02)00092-1).
- Hadley, P. K., A. Askar, and A. S. Cakmak. 1989. Scattering of waves by inclusions in a nonhomogeneous elastic half space solved by boundary element methods. Technical Report: NCEER-89-0027.
- Hisada, Y. 1994a. An efficient method for computing Green's functions for a layered half-space with sources and receivers at close depths. *Bulletin of the Seismological Society of America* 84 (5): 1456–72.
- Hisada, Y. 1994b. An efficient method for computing Green's functions for a layered half-space with sources and receivers at close depths (Part 2). *Bulletin of the Seismological Society of America* 85 (4): 1080–93.
- Huang, L., Z. Liu, C. Wu, and J. Liang. 2019. The scattering of plane *P*, *SV*-waves by twin lining tunnels with imperfect interfaces embedded in an elastic half-space. *Tunnelling and Underground Space Technology* 85: 319–30. doi: [10.1016/j.tust.2018.12.024](https://doi.org/10.1016/j.tust.2018.12.024).
- Israil, A. S. M., and P. K. Banerjee. 1990a. Advanced development of time-domain BEM for two-dimensional scalar wave propagation. *International Journal for Numerical Methods in Engineering* 5 (29): 1003–20. doi: [10.1002/nme.1620290507](https://doi.org/10.1002/nme.1620290507).
- Israil, A. S. M., and P. K. Banerjee. 1990b. Advanced time-domain formulation of BEM for two-dimensional transient elastodynamics. *International Journal for Numerical Methods in Engineering* 29 (7): 1421–40. doi: [10.1002/nme.1620290704](https://doi.org/10.1002/nme.1620290704).

- Jalali, R. S., Z. Tokmechi, and M. D. Trifunac. 2015. A note on the surface motion of a semi-cylindrical alluvial valley for incident-cylindrical *SH* waves radiating from a fault with arbitrary orientation. *Soil Dynamics and Earthquake Engineering* 79 (A): 80–88. doi: [10.1016/j.soildyn.2015.08.002](https://doi.org/10.1016/j.soildyn.2015.08.002).
- Kamalian, M., B. Gatmiri, A. Sohrabi-Bidar, and A. Khalaj. 2007. Amplification pattern of 2D semi-sine shaped valleys subjected to vertically propagating incident waves. *Communications in Numerical Methods in Engineering* 23 (10): 871–87. doi: [10.1002/cnm.933](https://doi.org/10.1002/cnm.933).
- Kawase, H. 1988. Time-domain response of a semi-circular canyon for incident *SV*, *P* and *Rayleigh*-waves calculated by the discrete wave-number boundary element method. *Bulletin of the Seismological Society of America* 78 (4): 1415–37.
- Kawase, H., and T. Sato. 1992. Simulation analysis of strong motions in the Ashigara valley considering one- and two-dimensional geological structures. *Journal of Physics of the Earth* 40: 27–56. doi: [10.4294/jpe1952.40.27](https://doi.org/10.4294/jpe1952.40.27).
- Keller, J. B. 1962. Geometrical Theory of Diffraction. *Journal of the Optical Society of America* 52 (2): 116–30. doi: [10.1364/JOSA.52.000116](https://doi.org/10.1364/JOSA.52.000116).
- Komatitsch, D., and J. P. Vilotte. 1998. The spectral element method: An efficient tool to simulate the seismic response of 2D and 3D geological structures. *Bulletin of the Seismological Society of America* 88: 368–92.
- Le, T., V. W. Lee, and M. D. Trifunac. 2017. *SH* waves in a moon-*SH*aped valley. *Soil Dynamics and Earthquake Engineering* 101: 162–75. doi: [10.1016/j.soildyn.2017.06.019](https://doi.org/10.1016/j.soildyn.2017.06.019).
- Lee, V. W. 1984. Three-dimensional diffraction of plane *P*, *SV* & *SH*-waves by a hemispherical alluvial valley. *Int J Soil Dyn Earthq Eng* 3 (3): 199–144.
- Liang, J., Z. Liu, L. Huang, and G. Yang. 2019. The indirect boundary integral equation method for the broadband scattering of plane *P*, *SV* and *Rayleigh* waves by a hill topography. *Engineering Analysis with Boundary Elements* 98: 184–202. doi: [10.1016/jenganabound.2018.09.018](https://doi.org/10.1016/jenganabound.2018.09.018).
- Liu, Z., L. Huang, J. Liang, and C. Wu. 2019. A three-dimensional indirect boundary integral equation method for modeling elastic wave scattering in a layered half-space. *International Journal of Solids and Structures* 169: 81–94. doi: [10.1016/j.ijsolstr.2019.03.020](https://doi.org/10.1016/j.ijsolstr.2019.03.020).
- Lubich, C. 1988. Convolution quadrature and discretized operational calculus. I. *Numerische Mathematik* 52 (2): 129–145.
- Luco, J. E., and F. C. P. De Barros. 1994. Dynamic displacements and stresses in the vicinity of a cylindrical cavity embedded in a half-space. *Earthquake Engineering & Structural Dynamics* 23 (3): 321–40. doi: [10.1002/eqe.4290230307](https://doi.org/10.1002/eqe.4290230307).
- Luco, J. E., H. L. Wong, and F. C. P. De Barros. 1990. Three-dimensional response of a cylindrical canyon in a layered half-space. *Earthquake Engineering & Structural Dynamics* 19 (6): 799–817. doi: [10.1002/eqe.4290190603](https://doi.org/10.1002/eqe.4290190603).
- Luco, J. E., and R. J. Apsel. 1983a. On the Green's functions for a layered half-space. Part I. *Bulletin of the Seismological Society of America* 73 (4): 909–29.
- Luco, J. E., and R. J. Apsel. 1983b. On the Green's functions for a layered half-space. Part I. *Bulletin of the Seismological Society of America* 73 (4): 931–51.
- Lysmer, J., and L. A. Drake. 1972. A finite element method for seismology. *Methods of Computational Physics*, Ed Bolt BA, Academic Press, New York. 11: 181–216.
- Manolis, G. D., P. S. Dineva, T. V. Rangelov, and F. Wuttke. 2017. *Seismic wave propagation in non-homogeneous elastic media by boundary elements*. Springer: Series, Solid Mechanics and Its Applications, 294. doi:[10.1007/978-3-319-45206-7](https://doi.org/10.1007/978-3-319-45206-7)
- Manoogian, M. E. 1992. Scattering and diffraction of plane *SH*-waves by surface and subsurface topography of arbitrary shape. Ph.D. diss., USA: University of southern California.
- Manoogian, M. E., and V. W. Lee. 1999. Antiplane deformations near arbitrary-shape alluvial valleys. *ISSET Journal of Earthquake Technology* 36 (2): 107–20.
- MATLAB. 2019. *The language of technical computing*. V. 9.7. Natick, MA: The MathWorks Inc.
- Moczó, P., and P. Y. Bard. 1993. Wave diffraction, amplification and differential motion near strong lateral discontinuities. *Bulletin of the Seismological Society of America* 83: 85–106.
- Najafzadeh, J., M. Kamalian, M. K. Jafari, and N. Khaji. 2014. Seismic analysis of rectangular alluvial valleys subjected to incident *SV*-waves using the spectral finite element method. *International Journal of Civil Engineering* 12: 251–63.
- Nohegoo-Shahvari, A., M. Kamalian, and M. Panji. 2018. Two-dimensional dynamic analysis of alluvial valleys subjected to vertically propagating incident *SH*-waves. *International Journal of Civil Engineering*. doi: [10.1007/s40999-018-0369-x](https://doi.org/10.1007/s40999-018-0369-x).
- Nohegoo-Shahvari, A., M. Kamalian, and M. Panji. 2019. A hybrid time-domain half-plane FE/BE approach for *SH*-wave scattering of alluvial sites. *Engineering Analysis with Boundary Elements* 105: 194–206. doi: [10.1016/jenganabound.2019.04.020](https://doi.org/10.1016/jenganabound.2019.04.020).
- Panji, M. 2013. Seismic analysis of topographic features subjected to *SH*-waves by a half-Plane time-domain BEM. PhD diss., Tehran, Iran: Islamic Azad University Science and Research Branch.
- Panji, M., and B. Ansari. 2017a. Modeling pressure pipe embedded in two-layer soil by a half-plane BEM. *Computers and Geotechnics* 81 (C): 360–67. doi: [10.1016/j.compgeo.2016.09.006](https://doi.org/10.1016/j.compgeo.2016.09.006).
- Panji, M., and B. Ansari. 2017b. Transient *SH*-wave scattering by the lined tunnels embedded in an elastic half-plane. *Engineering Analysis with Boundary Elements* 84: 220–30.

- Panji, M., H. Koohsari, M. Adampira, H. Alielahi, and J. Asgari Marnani. 2016. Stability analysis of shallow tunnels subjected to eccentric loads by a boundary element method. *Journal of Rock Mechanics and Geotechnical Engineering* 8 (4): 480–88. doi: [10.1016/j.jrmge.2016.01.006](https://doi.org/10.1016/j.jrmge.2016.01.006).
- Panji, M., J. Asgari Marnani, and S. Tavousi Tafreshi. 2011. Evaluation of effective parameters on the underground tunnel stability using BEM. *Journal of Structural Engineering and Geo-Techniques* 1 (2): 29–37.
- Panji, M., M. Kamalian, J. Asgari Marnani, and M. K. Jafari. 2013a. Transient analysis of wave propagation problems by half-plane BEM. *Geophysical Journal International* 194 (3): 1849–65. doi: [10.1093/gji/ggt200](https://doi.org/10.1093/gji/ggt200).
- Panji, M., M. Kamalian, J. Asgari Marnani, and M. K. Jafari. 2013b. Amplification pattern of semi-sine shaped valleys subjected to vertically propagating incident SH-waves. Computational Methods in Engineering. Isfahan, Iran: Isfahan University of Technology (IUT).
- Panji, M., M. Kamalian, J. Asgari Marnani, and M. K. Jafari. 2014a. Analysing seismic convex topographies by a half-plane time-domain BEM. *Geophysical Journal International* 197 (1): 591–607. doi: [10.1093/gji/ggu012](https://doi.org/10.1093/gji/ggu012).
- Panji, M., M. Kamalian, J. Asgari Marnani, and M. K. Jafari. 2014b. Antiplane seismic response from semi-sine shaped valley above embedded truncated circular cavity: A time-domain half-plane BEM. *International Journal of Civil Engineering* 12 (2 and B): 160–73.
- Panji, M., and S. Mojtabazadeh Hasanlouei. 2018. Time-history responses on the surface by regularly distributed enormous embedded cavities: Incident SH-waves. *Earthquake Science* 31: 1–17.
- Panji, M., and S. Mojtabazadeh-Hasanlouei. 2019a. Seismic amplification pattern of the ground surface in presence of twin unlined circular tunnels subjected to SH-waves [In Persian]. *Journal Transportation Infrastructure Engineering*. doi: [10.22075/jtie.2019.16056.1342](https://doi.org/10.22075/jtie.2019.16056.1342).
- Panji, M., and S. Mojtabazadeh-Hasanlouei. 2019b. Transient response of irregular surface by periodically distributed semi-sine shaped valleys: Incident SH-waves. *Journal of Earthquake Tsunami*. doi: [10.1142/S1793431120500050](https://doi.org/10.1142/S1793431120500050).
- Panji, M., S. Mojtabazadeh-Hasanlouei, and F. Yasemi. 2020. A half-plane time-domain BEM for SH-wave scattering by a subsurface inclusion. *Computers & Geosciences* 134: 104342. doi: [10.1016/j.cageo.2019.104342](https://doi.org/10.1016/j.cageo.2019.104342).
- Paolucci, R. 2002. Amplification of earthquake ground motion by steep topographic irregularities. *Earthquake Engineering & Structural Dynamics* 31 (10): 1831–53. doi: [10.1002/eqe.192](https://doi.org/10.1002/eqe.192).
- Rajapakse, R. K. N. D., and Y. Wang. 1993. Green's functions for transversely isotropic elastic half-space. *Journal of Engineering Mechanics* 119 (9): 1724–46. doi: [10.1061/\(ASCE\)0733-9399\(1993\)119:9\(1724\)](https://doi.org/10.1061/(ASCE)0733-9399(1993)119:9(1724)).
- Reinoso, E., L. C. Wrobel, and H. Power. 1993. Preliminary results of the modelling of the Mexico City valley with a two-dimensional boundary element method for the scattering of SH waves. *Soil Dynamics and Earthquake Engineering* 12 (8): 457–68. doi: [10.1016/0267-7261\(93\)90030-U](https://doi.org/10.1016/0267-7261(93)90030-U).
- Ricker, N. 1953. The form and laws of propagation of seismic wavelet. *Geophysics* 18 (1): 10–40. doi: [10.1190/1.1437843](https://doi.org/10.1190/1.1437843).
- Sánchez-Sesma, F. J. 1987. Site effects on strong ground motion. *Soil Dynamics and Earthquake Engineering* 6 (2): 124–32. doi: [10.1016/0267-7261\(87\)90022-4](https://doi.org/10.1016/0267-7261(87)90022-4).
- Sánchez-Sesma, F. J., and E. Rosenblueth. 1979. Ground motion at canyons of arbitrary SHape under incident SH waves. *Earthquake Engineering & Structural Dynamics* 7: 441–50. doi: [10.1002/eqe.4290070505](https://doi.org/10.1002/eqe.4290070505).
- Sánchez-Sesma, F. J., and F. Luzon. 1995. Seismic response of three-dimensional alluvial valleys for incident P, S and Rayleigh-waves. *Bulletin of the Seismological Society of America* 85 (1): 269–84.
- Sánchez-Sesma, F. J., and J. A. Esquivel. 1979. Ground motion on alluvial valleys under incident plane SH-waves. *Bulletin of the Seismological Society of America* 69: 1107–20.
- Sánchez-Sesma, F. J., V. J. Palencia, and F. Luzón. 2002. Estimation of local site effects during earthquakes: An overview. *ISSET Journal of Earthquake Technology* 39 (3): 167–93.
- Senjuntichai, T., and R. K. N. D. Rajapakse. 1994. Dynamic Green's functions of homogeneous poroelastic half-plane. *Journal of Engineering Mechanics* 120 (11): 2381–404. doi: [10.1061/\(ASCE\)0733-9399\(1994\)120:11\(2381\)](https://doi.org/10.1061/(ASCE)0733-9399(1994)120:11(2381)).
- Sherif, R. I., and V. W. Lee. 1996. Diffraction around a circular alluvial valley in an elastic wedge-shaped medium due to plane SH-waves. *European Earthquake Engineering* 3: 21–28.
- Smith, W. D. 1975. The application of finite element analysis to body wave propagation problems. *Geophysical Journal of the Royal Astronomical Society* 42 (2): 747–68. doi: [10.1111/j.1365-246X.1975.tb05890.x](https://doi.org/10.1111/j.1365-246X.1975.tb05890.x)
- Takemiya, H., and A. Fujiwara. 1994. SH-wave scattering and propagation analyses at irregular sites by time-domain BEM. *Bulletin of the Seismological Society of America* 84 (5): 1443–55.
- Todorovska, M. I., and V. W. Lee. 1991. Surface motion of shallow circular alluvial valleys for incident plane SH-waves (Analytical solution). *Soil Dynamics and Earthquake Engineering* 10 (4): 192–200. doi: [10.1016/0267-7261\(91\)90033-V](https://doi.org/10.1016/0267-7261(91)90033-V).
- Trifunac, M. D. 1971. Surface motion of a semi-cylindrical alluvial valley for incident plane SH-waves. *Bulletin of the Seismological Society of America* 61 (6): 1755–70.
- Trifunac, M. D. 1973. Scattering of plane SH waves by a semi-cylindrical canyon. *Earthquake Engineering & Structural Dynamics* 1: 267–81. doi: [10.1002/eqe.4290010307](https://doi.org/10.1002/eqe.4290010307).
- Tsaur, D. H., and K. H. Chang. 2008a. SH-waves scattering from a partially filled semi-circular alluvial valley. *Geophysical Journal International* 173 (1): 157–67. doi: [10.1111/j.1365-246X.2007.03581.x](https://doi.org/10.1111/j.1365-246X.2007.03581.x).
- Tsaur, D. H., and K. H. Chang. 2009. Scattering of SH-waves by truncated semi-cylindrical canyon. *Journal of Engineering Mechanics*, ASCE. 135: 862–70. doi: [10.1061/\(ASCE\)0733-9399\(2009\)135:8\(862\)](https://doi.org/10.1061/(ASCE)0733-9399(2009)135:8(862)).

- Tsaur, D. H., and K. H. Chang. 2018. Exact solution to scattering of *SH* waves by an elliptic-arc canyon in the corner of an elastic quarter space. *Soil Dynamics and Earthquake Engineering* 110: 137–40. doi: [10.1016/j.soildyn.2018.02.016](https://doi.org/10.1016/j.soildyn.2018.02.016).
- Wang, L., Y. Xu, J. Xia, and Y. Luo. 2015. Effect of near-surface topography on high-frequency *Rayleigh*-wave propagation. *Journal of Applied Geophysics* 116: 93–103. doi: [10.1016/j.jappgeo.2015.02.028](https://doi.org/10.1016/j.jappgeo.2015.02.028).
- Weihua, L., Z. Chenggang, and S. Peixin. 2005. Scattering of plane *P*-waves by circular-arc alluvial valleys with saturated soil deposits. *Soil Dynamics and Earthquake Engineering* 25 (12): 997–1014. doi: [10.1016/j.soildyn.2004.10.010](https://doi.org/10.1016/j.soildyn.2004.10.010).
- Wong, H. L., and M. D. Trifunac. 1974a. Surface motion of a semi-elliptical alluvial valley for incident plane *SH*-waves. *Bulletin of the Seismological Society of America* 64 (5): 1389–408.
- Wong, H. L., and M. D. Trifunac. 1974b. Scattering of plane *SH*-waves by a semi-elliptical canyon. *Earthquake Engineering & Structural Dynamics* 3 (2): 157–69. doi: [10.1002/eqe.4290030205](https://doi.org/10.1002/eqe.4290030205).
- Yuan, X., and Z. Liao. 1995. Scattering of plane *SH*-waves by a cylindrical alluvial valley of circular-arc cross-section. *Earthquake Engineering & Structural Dynamics* 24 (10): 1303–13. doi: [10.1002/eqe.4290241002](https://doi.org/10.1002/eqe.4290241002).
- Zhang, N., Y. Gao, and R. Y. S. Pak. 2017. Soil and topographic effects on ground motion of a surficially inhomogeneous semi-cylindrical canyon under oblique incident *SH*-waves. *Soil Dynamics and Earthquake Engineering* 95: 17–28. doi: [10.1016/j.soildyn.2017.01.037](https://doi.org/10.1016/j.soildyn.2017.01.037).
- Zhang, N., Y. Gao, Y. Cai, D. Li, and Y. Wu. 2012. Scattering of *SH*-waves induced by a non-symmetrical V-shaped canyon. *Geophysical Journal International* 191 (1): 243–56. doi: [10.1111/j.1365-246X.2012.05604.x](https://doi.org/10.1111/j.1365-246X.2012.05604.x).
- Zhang, W., and X. F. Chen. 2006. Traction image method for irregular free-surface boundaries in finite difference seismic wave simulation. *Geophysical Journal International* 167 (1): 337–53. doi: [10.1111/j.1365-246X.2006.03113.x](https://doi.org/10.1111/j.1365-246X.2006.03113.x).
- Zhou, H., and X. F. Chen. 2006. A new approach to simulate scattering of *SH*-waves by an irregular topography. *Geophysical Journal International* 164: 449–59. doi: [10.1111/j.1365-246X.2005.02670.x](https://doi.org/10.1111/j.1365-246X.2005.02670.x).